# Hydro-climatic drivers of land-based micropollutant fluxes: the regime of the largest river water inflow of the Mediterranean Sea

Hugo Delile, Matthieu Masson, Cécile Miège, Jérôme Le Coz, Gaelle Poulier, Chloe Le Bescond, Olivier Radakovitch, Marina Coquery

# Hydro-climatic drivers of land-based organic and inorganic particulate-bound micropollutant fluxes: the regime of the largest river water inflow of the Mediterranean Sea

**Authors:** Hugo Delile[1*], Matthieu Masson[1], Cécile Miège[1], Jérôme Le Coz[1], Gaëlle Poulier[1], Chloé Le Bescond[1], Olivier Radakovitch[2,3], Marina Coquery[1]

[1]INRAE, UR RiverLy, 5 rue de la Doua CS 20244, F-69625 Villeurbanne, France

[2]Institut de Radioprotection et de Sûreté Nucléaire (IRSN), PSE-ENV/SRTE/LRTA, BP3, 13115 Saint-Paul Lez Durance, France

[3]Aix Marseille Univ, CNRS, IRD, INRA, Coll France, CEREGE, Aix-en-provence, France.

*Corresponding author: hugo.delile@irstea.fr

## Abstract

Land-based micropollutants are the largest pollution source of the marine environment acting as the major large-scale chemical sink. Despite this, there are few comprehensive datasets for estimating micropollutant fluxes released to the sea from river mouths. Hence, their dynamics and drivers remain poorly understood. Here, we address this issue by continuous measurements throughout the Rhône River basin (~ 100,000 km²) of 1) particulate-bound micropollutant concentrations (persistant organic micropollutants: polychlorobiphenyls [PCBi] and polycyclic aromatic hydrocarbons [PAHs]; emerging compounds: glyphosate and AMPA; and trace metal elements [TME]), 2) suspended particulate matter [SPM], and 3) water discharge. From these data, we computed daily fluxes for a wide range of micropollutants ($n$ = 29) over a long-term period (2008-2018). We argue that almost two third of annual micropollutant fluxes is released to the Mediterranean Sea during three short-term periods over the year. The watershed hydro-climatic heterogeneity determines this dynamic

by triggering seasonal floods. Unexpectedly, the large deficit of the inter-annual monthly micropollutant fluxes inputs (tributaries and the Upper Rhône River) compared to the output (Beaucaire station) claims for highly contaminated missing sources of micropollutants in the Rhône River watershed. Based on a SPM-flux-averaged micropollutant concentrations mass balance of the system and the estimates of the relative uncertainty of the missing source concentration, we assessed their location within the Rhône River catchment. We assume that the potential missing sources of PAHs, PCBi and TME (only for Pb, Cd and Hg) would be, respectively, the metropolitan areas and the alluvial margins of the Rhône River valley, and the unmonitored Cevenol tributaries.

**Keywords**: Particulate micropollutant fluxes, Suspended particulate matter, Rhône River, Mediterranean Sea, Hydrological dynamic, Land-based pollution

## 1. Introduction

Identified as one of the nine processes that regulate the stability and resilience of the Earth system, chemical pollution and its control variables, and interactions with other biophysical processes, remains poorly quantified (Rockström et al., 2009; Steffen et al., 2015; Lade et al., 2019). Such quantification is all the more critical as the large-scale ubiquity of chemical pollution threats at least half of European freshwater bodies (Malaj et al., 2014). Organic micropollutants and trace metal elements (TME) are released into the hydrographic networks from agricultural, industrial, domestic and mining activities, and urban areas (Meybeck et al., 2003). They are largely transferred downstream and finally trapped into the marine environment. As a result, land-based human activities are known to be the largest source of pollution to the marine environment, which act as the major chemical sink at the regional and global scales (Dachs et al., 2002; Gioia et al., 2011). Source-to-sink transport of micropollutants are river mouths for the coastal environments and atmosphere for the open

ocean (Gioia et al., 2011; Gómez-Gutiérrez et al., 2006; Wang et al., 2007; Liu et al., 2008). In fact, an undetermined amount of the micropollutants discharged into the coastal environments is then transferred through unknown routes to open seawaters, thus acting as an additional source of contamination to the remote marine environment (Gioia et al., 2011).

Persistent organic pollutants (POPs), such as indicator polychlorobiphenyls (PCBi) and polycyclic aromatic hydrocarbons (PAHs), and most TME are preferentially transported on suspended particulate matter (SPM) (Meyer et al., 2009; Schwientek et al., 2013). In rivers, SPM are (i) providing an integrated signal of particle-bound micropollutant concentrations (Schwientek et al., 2013; Masson et al., 2018; Rügner et al., 2019), and (ii) acting as the main transfer driver of such micropollutants into the river networks (UNEP/MAP, 2003; Horowitz et al., 2009). Therefore, the accurate assessment of SPM-bound micropollutant transported and discharged by rivers is critical to appraise the environmental and health risks they pose, as well as to develop suitable management programs for limiting them (Gómez-Gutiérrez et al., 2006; Walling et al., 2003). Unfortunately, our current knowledge on micropollutant fluxes transferred to the sea via the main rivers of the globe is insufficient, as is their seasonal dynamics (i.e., Gómez-Gutiérrez et al., 2006; Qi et al., 2014; Parajulee et al., 2017; Launay et al., 2019; Poulier et al., 2019). This is largely due to the difficulty to obtain, over a large period of time, all the data required to calculate micropollutant fluxes, including comprehensive datasets on water discharge, SPM and particulate micropollutant concentrations (Ollivier et al., 2011; Poulier et al., 2019). Actually, the assessment of the total sediment fluxes delivery to the sea, for which the suspended sediment load largely prevails compared to the bedload load (Syvitski and Saito, 2007), is not widespread since less than 10% of the river mouths worldwide have been monitored for their sediment delivery (Syvitski et al., 2005; Bravard, 2018). Such a monitoring within the river catchments is even rarer (Bravard, 2018). Moreover, available SPM concentration data are generally focused on a

particular event (typically flood) or over a limited period of time (typically one year), leading also to large uncertainties on the inter-annual average SPM and micropollutant fluxes estimations (Gómez-Gutiérrez et al., 2006; Wang et al., 2007; UNEP/MAP, 2003; Qi et al., 2014; Launay et al., 2019; Bravard, 2018). Finally, most studies lack representative dataset on micropollutant concentrations in SPM to calculate inter-annual average micropollutant fluxes in rivers, as this is a sampling and analytical challenge that remains expensive and labour intensive (Poulier et al., 2019).

The targeted hydrophobic organic micropollutants (PCBi and PAHs) are POPs (Tables S1 and S2), legacy contaminants, listed for PCBi in the Stockholm Convention (UNEP, 2001) and for PAHs in the Aarhus Protocol on Persistent Organic Pollutants (United Nations, 1998), because of their toxic, persistent, bioaccumulative, ubiquitous and lipophilic properties. We also focused on glyphosate and its degradation product aminomethylphosphonic acid (AMPA), as these emerging and absorbable organic micropollutants recently raised great concerns in our societies (e.g., Beckie et al., 2020). Indeed, the ubiquity of glyphosate and AMPA in the environment, and particularly in surface waters and sediments (Grandcoin et al., 2016), results from the extensively resort of the parent compound as the most effective herbicide used worldwide (e.g., Baylis, 2000; Grandcoin et al., 2016; Beckie et al., 2020). Because glyphosate and AMPA are strongly adsorbed to soil particles (hydrogen and cationic interactions; Al Rajab, 2007) (e.g., Grandcoin et al., 2016), they reach water streams through rainfall-induced runoff (e.g., Yang et al., 2015). This is all the more important to focus on these two compounds that there are very few studies dealing with the concentrations of glyphosate and AMPA in river sediments and even rarer on river fluxes. Finally, because this study aims to include a wide range of micropollutants, we spread our investigations to 9 TME. All these micropollutants are priority substances within the scope of European regulations (i.e., Water Framework Directive, E.C, 2000). For the first time, to our

knowledge, the present study investigated simultaneously the SPM-bound micropollutant concentrations and fluxes of 20 organic and 9 inorganic priority pollutants over ten years (2008-2018) at the Rhône River mouth, and on its main tributaries, covering 80% of the watershed area (~ 96,500 km²) (Fig. 1).

The main goal of this study is to decipher the major drivers controlling the transport and export of the micropollutant fluxes and concentrations from a large river basin into the sea. In this aim, we took into account the long-term character of our data set by calculating 10-years yearly and monthly averages. This investigation is based on time-integrative micropollutant concentrations, and continuous SPM and water discharge data acquired throughout the Rhône River catchment. This implies to (i) accurately quantify the inter-annual average fluxes of a large range of organic and inorganic micropollutants ($n$ = 29) released into the Mediterranean Sea, (ii) identify the specific contributions of the main Rhône River tributaries, (iii) explore the seasonal dynamics of the micropollutant fluxes within the Rhône River catchment and at its outlet, and (iv) determine the land-based chemical pollution sources.

## 2. Materials and Methods

### 2.1. Study area

We chose to focus specifically on the Rhône River based on the main features of this large river catchment (Fig. 1), which naturally places it as a reference for the assessment of SPM-bound micropollutant fluxes that are discharged into the Mediterranean Sea:

- The Rhône River is the largest single source of freshwater (~ 18% of the total inputs) (e.g., UNEP/MAP, 2003; Antonelli et al., 2008; Ludwig et al., 2009) and particulate matter (e.g., Qi et al., 2014; Antonelli et al., 2008; Syvitski et al., 2007) of the Mediterranean Sea;

- The Rhône River catchment is characterized by a land-use diversity (Fig. S1) and a high population density with ~ 180 inh/km² (one-third higher than the French average);

- The Rhône River catchment is characterized by a striking climatic and geological heterogeneity (e.g., Bethemont and Bravard, 2016; Launay et al., 2019). The northern part of the watershed is characterized by oceanic influences and the southern part by Mediterranean climatic conditions. The geological contrast of the Rhône River basin stretches from west to east, since its western edge corresponds to the old Hercynian crustal segments (240 Ma and older) of the Massif Central, and its eastern fringe is marked by the young Alpine mountains (30–120 Ma) (Blichert-Toft et al., 2016);

- The Rhône River is composed of three distinct hydrological regimes including snow and glacier melting (Isère River and the Upper Rhône), an oceanic pluvial regime (Saône River), and a Mediterranean component (Durance River).

## 2.2. SPM sampling

Except for the Rhône River at Beaucaire station, SPM samples were collected using particle traps designed with the same characteristics of those described in Schulze et al. (2007). The related technical features are detailed in Schulze et al. (2007), Masson et al. (2018), and Poulier et al. (2019). Particle traps were immersed near the riverbank in the water column at a depth of 0.5-1 m at cross-section with fairly homogeneous SPM concentrations (Launay, 2014). At each station, SPM sampling is done every month, but for the Upper Rhône River (Jons station) the particle trap was emptied every two weeks. Particulate traps accumulate a volume of suspended matter proportional to the SPM concentration in the water, which is the most variable parameter that makes the SPM flux (discharge varies over a much narrower range). Therefore, samples from particle traps are nearly proportional to SPM flux variations, not just time-averaged concentrations. They are therefore suitable for micropollutants fluxes assessment (Schulze et al., 2007; Masson et al., 2018). The use of particle traps allowed continuous sampling of SPM over the exposure time, as well as

recovering sufficient amounts of particles for micropollutant analysis. At the Beaucaire station, SPM samples for micropollutant analysis were collected every two weeks by a high speed continuous flow centrifuge (Masson et al., 2018; Poulier et al., 2019). The comparative study conducted by Masson et al. (2018) on the SPM sampling between particle traps and a continuous flow centrifuge did not show significant differences in Hg and PCB concentrations testifying that these SPM sampling systems are comparable. The particle size distributions of the SPM samples collected in the present study (i.e., for the six river stations investigated) are mainly multimodal. Indeed, between 2 and 4 (3 in most cases) Gaussian distributions were generally observed: mode 1 between 1 and 10 µm (average 4 µm particle size; clays and very fine silts), mode 2 between 10 and 27 µm (average 14 µm; fine silts), mode 3 between 27 and 80 µm (average 39 µm; coarse silts), and mode 4 between 80 and 2000 µm (average 136 µm; fine to coarse sands) (Launay, 2014; Masson et al., 2018; Lepage et al., 2019). The SPM samples were sorted depending on the hydrological conditions during SPM sampling, and the median micropollutants concentrations was calculated for low flow and flood conditions. These low flow or flood site-specific median concentrations were used to fill the gaps in the measurement time series, which resulted from field material vandalism, or technical and logistical glitches. In this respect, thresholds were defined at each station to distinguish hydrological regimes with potentially differing contamination levels. The rule is as follows: if more than 50% of the SPM cumulative flux over the exposure period of the particle trap corresponds to a water discharge higher than the flood threshold (defined as half of the 2-year flood peak discharge), then the SPM samples are considered under flood conditions. By doing so, we obtained low flow and flood median concentrations for all micropollutants at each station (Table S2).

### 2.3. Water discharges

172 Hourly averaged water discharge data at each station, except for the Rhône River at Jons
173 station for which no hydrometric station exists, were provided by the "*Compagnie Nationale*
174 *du Rhône*" (CNR), the main operator of hydropower plant on the Rhône River. At the Jons
175 station, hourly water discharge was computed using a 1-D hydrodynamical model (Launay et
176 al., 2019), requiring the discharge data of the Rhône River at Lagnieu, and those from the Ain
177 and the Bourbre tributaries.

178 **2.4. SPM concentrations**

179 The method for the estimation of SPM concentrations is described in detail in Poulier et al.
180 (2019), and the main steps are summarized here. Except for the Rhône River at Arles, SPM
181 concentrations are derived from *in situ* turbidity measurements every 10 min, and
182 reconstituted via site-specific turbidity-SPM rating curves calibrated using water sampling
183 and filtration (i.e., by manual water sample collection at the time of SPM sampling, and by
184 automated hourly sampling during flood events). At Arles solely, daily time-integrated SPM
185 concentrations were measured, and used for the fluxes computed at Beaucaire. We considered
186 that it was representative for both branches of the Rhône River, as fine particle inputs are
187 negligible between the two stations (Pont et al., 2002). For low flow conditions,
188 concentrations of SPM were obtained by analysis of daily composite water samples collected
189 automatically, whereas during floods the sampling frequency was increased to every 4 h for a
190 better temporal resolution. Data are freely available from the online database of the Rhône
191 Sediment Observatory (Thollet et al., 2018).

192 **2.5. Micropollutant concentrations**

193 **2.5.1. Polychlorobiphenyls (PCBi) analysis**

194 The concentrations of 7 indicator PCBi (congeners 28, 52, 101, 118, 138, 153, and 180) in
195 SPM were analyzed by IRSTEA laboratory according to the French Standard XP X33-012

196 (AFNOR, 2000). Approximately 1.0 g dry weight (d.w.) of sample was extracted with a
197 cyclohexane/acetone 90:10 v/v mixture, concentrated by evaporation and purified on a 1 g
198 Florisil SPE cartridge. A small amount of copper powder (10 mg $mL^{-1}$) was finally added in
199 order to avoid sulfur interferences prior to gas chromatography analysis with a $^{63}Ni$ electron
200 capture detector (GC-ECD). Samples were analyzed on two different columns (RTX®-5, 30
201 m × 0.25 mm × 0.25 µm for quantification and RTX®-PCB, 30 m× 0.25 mm× 0.25 µm for
202 confirmation of the compound identity) to confirm the results. Procedural blanks and control
203 standard solutions were systematically checked. The accuracy of measurements was checked
204 via intercomparison exercises and the analysis of a certified reference material (BCR 536). A
205 sediment sample from the Bourbre River, a tributary of the Rhône River, was used to
206 determine analytical uncertainties, as no certified reference material exists for such low levels
207 of PCBi in equivalent matrix. Analytical uncertainties were estimated to be 60% (k = 2) for
208 concentrations lower than 3-times the limit of quantification (LOQ) and to be 30% (k = 2) for
209 concentrations higher than 3-times the LOQ. The LOQs were estimated between 0.5 and 1 µg
210 $kg^{-1}$ (d.w.) depending on the congeners. PCBi 28 and 52 were mostly below the LOQ
211 (average quantification frequency around 35%), and were not used in this study. The
212 quantification frequency (QF) of the other congeners was on average 72%. Data are freely
213 available from the online database of the Rhône Sediment Observatory (Thollet et al., 2018).
214

215 **2.5.2. Polycyclic aromatic hydrocarbons (PAHs) analysis**

216 A total of 15 priority PAHs (2-methylfluoranthene, anthracene, benz[a]anthracene,
217 benzo[a]pyrene, benzo[b]fluoranthene, benzo[ghi]perylene, benzo[k]fluoranthene, chrysene,
218 dibenz[a,h]anthracene, fluoranthene, indeno[1,2,3-cd]pyrene, phenanthrene, pyrene,
219 naphtalene and 2-methynaphtalene) were analyzed by the accredited Laboratory of Hygiene
220 and Environment (Alpha group, Rouen, France) according to the XP X33-012 Standard

(AFNOR, 2000). Samples were extracted with a hexane/acetone 50:50 v/v mixture, concentrated by evaporation and purified on silica, then analyzed by capillary gas chromatography coupled to a mass spectrometer (GC-MS). Analytical uncertainties were estimated to be 60% (k = 2) for concentrations lower than 3-times the LOQ and to be 30% (k = 2) for concentrations higher than 3-times the LOQ. The LOQ ranged from 1 to 2 µg $kg^{-1}$ (d.w.) for most of the PAHs, except for dibenz[a,h]anthracene and phenanthrene (up to 5 µg $kg^{-1}$). Naphtalene and 2-methynaphtalene were mostly below the LOQ (average QF around 50%) and were not used in this study. The QF of the other PAHs was on average 96%. The laboratory was accredited by the French Committee for Accreditation (Cofrac) (accreditation n° 1-1351) for measuring PAHs in sediments and fulfils the requirements of the standard NF EN ISO/IEC 17025 (2017).

### 2.5.3. Glyphosate and AMPA analysis

Glyphosate and AMPA were analyzed by the accredited Laboratory of Hygiene and Environment (Alpa group, Rouen, France). Extraction was performed by agitation with an alkaline solution of 0.5M KOH. Then, a SPE purification step was carried out using an Oasis HLB cartridge. Before analysis, a derivation step was achieved (with 9-fluorenylmethylchloroformate). The analysis was done by capillary liquid chromatography coupled to a mass spectrometer (LC-MS). The LOQ of glyphosate and AMPA for a 5 g (d.w.) sample ) was 10 µg $kg^{-1}$ (d.w.). The QF was on average 55% for glyphosate and 86% for AMPA. The laboratory was accredited by the French Committee for Accreditation (Cofrac) (accreditation n° 1-1351) for measuring glyphosate and AMPA in sediments and fulfils the requirements of the standard NF EN ISO/IEC 17025 (2017).

### 2.5.4. Trace Metal Elements (TME) and mercury (Hg) analysis

244 The TME (As, Cd, Co, Cr, Cu, Ni, Pb, Zn) in the SPM were measured by CEREGE
245 laboratory. Aliquots of 40-mg dry SPM were weighed out into acid-cleaned Teflon beakers.
246 All reagents were ultrapure grade compounds. Then, aliquots were dissolved in a mixture of 3
247 mL of HCl (34%), 4 mL $HNO_3$ (67%), 20 drops of $H_2O_2$ (35%) and 0.5 mL of HF (47-51%).
248 The mixtures were digested on a hotplate at 170°C (10 min), and then 250°C (10 min; P=100
249 bar) in an UltraWAVE Single Reaction Chamber (Milestone, Thermo-Scientific). The
250 samples in solution were all clear, attesting the complete breakdown of the SPM samples. The
251 solutions were diluted with ultrapure Milli-Q water (Merck) and measured by ICP-MS
252 (Perkin-Elmer, Nexlon 300X) against calibration curves and rhodium solution as internal
253 standard. The procedural blanks and reference sediments STSD-3 and MESS-4 (Canadian
254 Certified Reference Materials Project) were analyzed repeatedly. Uncertainties for Cd, Co, Cr,
255 Cu, Ni, Pb, Zn and As concentration measurements were 14%, 3.6%, 1.2%, 5.0%, 2.3%,
256 3.2%, 3.0% and 6.7%, respectively. The LOQ of Cd, Co, Cr, Cu, Ni, Pb, Zn and As in SPM
257 were 0.1 mg $kg^{-1}$ (d.w.), 0.05 mg $kg^{-1}$ (d.w.), 0.1 mg $kg^{-1}$ (d.w.), 0.1 mg $kg^{-1}$ (d.w.), 1 mg $kg^{-1}$
258 (d.w.), 1 mg $kg^{-1}$ (d.w.), 5 mg $kg^{-1}$ (d.w.) and 0.5 mg $kg^{-1}$ (d.w.), respectively. The QF of all
259 TME was 100%.

260 The determination of total Hg in SPM was performed by IRSTEA laboratory using an
261 automated atomic absorption spectrophotometer, DMA 80 (Milestone), according to EPA
262 method 7473 (U.S. EPA, 1998). Blanks and certified reference materials (IAEA 433, marine
263 sediment; IAEA 457, coastal sediment; LGC 6187, river sediment) were systematically used
264 to control analytical accuracy (94%) and uncertainty (14%; k=2). The LOQ of Hg in SPM
265 was 10 µg $kg^{-1}$ (d.w.). Mercury was always quantified.

266 In the present paper, TME (including Hg) concentrations and fluxes were summed as
267 $\Sigma_9$TME to simplify the description of results, and thus facilitate the comparison of the TME
268 group with the other micropollutant families. Obviously, each TME or group of TME is

discussed apart since Zn and Cr weigh around two thirds of $\Sigma_9$TME (Table S1 and S2). Data are freely available from the online database of the Rhône Sediment Observatory (Thollet et al., 2018).

## 2.6. SPM and micropollutant fluxes

The calculation of SPM and micropollutant fluxes is based on the method developed in Poulier et al. (2019), and the main steps are summarized below. To appraise micropollutant fluxes at an inter-annual and inter-annual monthly resolution over the 2008-2018 exposure period, we calculated firstly SPM fluxes as the product of hourly measured data of both water discharges and SPM concentrations at each station. When missing values of SPM concentrations occurred (non-monitored periods or gaps in the measurement time series), SPM values were reconstructed on the basis of the empirical known relation involving water discharges (*Q*), and SPM concentrations (*Cs*) called *Cs*-*Q* rating curves (i.e., Poulier et al., 2019; Horowitz, 2003; Sadaoui et al., 2016). Secondly, micropollutant fluxes were calculated by multiplying the SPM fluxes to the monthly time-integrated particulate micropollutant concentrations obtained from particle traps, or by a continuous flow centrifuge only at the Rhône at Beaucaire station. Data for micropollutants with a QF< 50% were not considered in this study (2 PCBi and 2 PAHs). For some other organic micropollutants (other PCBi and PAHs), below LOQ data were changed to LOQ/2 for calculation.

Non-monitored periods or gaps in the measurement time series, which resulted from field material vandalism, or technical and logistical glitches, were filled by low flow or flood site-specific median concentrations for all micropollutants (Poulier et al., 2019). Because no micropollutant concentrations-water discharge relationships were found (Pearson's r between averaged water discharge and Hg, Pb, $\Sigma_{13}$PAH, $\Sigma_5$PCB, glyphosate and AMPA concentrations of -0.25, -0.16, 0.37, -0.15, 0.19 and -0.40, respectively at the Rhône River outlet) (Fig. S2),

we chose to fill gaps by the median of low flow or flood site-specific concentrations in order to be as close as possible to the field sampling condition based on time-integrated particle traps. In other words, this gap-filling technique provides the convenience of filling monthly average concentrations, rather than the detailed dynamics of instantaneous concentrations. Moreover, it is not useful to resort to continuous relationships, which do not really exist with respect to figure S2.

Accordingly, we distinguished the measured and the estimated micropollutant concentrations, depending on the availability of measurements from sediment-trap samples for the considered period. The total micropollutant flux ($F_{i,j}$) is the sum of the measured flux ($F_{i,j,\text{measured}}$) and the estimated flux ($F_{i,j,\text{estimated}}$) for which the micropollutant concentrations ($C_{i,j}$) are estimated (i.e., as the low flow and flood site-specific median concentrations). The total uncertainties of the inter-annual and inter-annual monthly micropollutant fluxes were estimated (distinguishing measured and estimated fluxes) using 95% level of uncertainty, which corresponds to 2 standard deviations for a Gaussian distribution; they are shown in absolute and relative values in Table S1 (see details on uncertainty computation in the supplementary text). We also computed the weight (in variance) of the estimated concentration uncertainty in the total flux uncertainty ($W_{i,j,\text{estimate}}$) (Table S1) (see the supplementary text). The uncertainty analysis we introduce in this paper, although via a simplified approach, proves to be an interesting exercise to assess the significance of our flux estimates.

## 3. Results and Discussion

### 3.1. Decadal assessment of inter-annual SPM and particulate micropollutant fluxes

316 For the period 2008-2018, we obtained an inter-annual average for $\Sigma_{13}$PAH, $\Sigma_5$PCB, $\Sigma_9$TME,
317 glyphosate and AMPA fluxes of about, respectively, 3.0±0.7 t $yr^{-1}$, 61±8 kg $yr^{-1}$, 1,802±152 t
318 $yr^{-1}$, 97±20 kg $yr^{-1}$, 220±45 kg $yr^{-1}$ at the Rhône River mouth (Beaucaire station) (Table S1).
319 The average of the total inter-annual fluxes uncertainty of the micropolluant families at the
320 same station is about 16% (ranging from 8 to 22% for, respectively, TME and PAHs) (Table
321 S1) for which the weight of the estimated concentration uncertainty accounts for about 46%
322 on average (ranging from 10 to 82% for, respectively, TME and glyphosate/AMPA) (Table
323 S1). The uncertainty analysis we introduce in this study proves to be an interesting way to
324 assess the reliability of our flux estimates. However, the total flux uncertainty and the weight
325 of the estimated concentration uncertainty in the total flux uncertainty show a high variability
326 according to the tributaries and the micropollutants considered (Table S1).

327 These estimates of the inter-annual average micropollutant fluxes are substantially
328 different from those found in the literature about organic and inorganic micropollutant fluxes
329 discharged by the Rhône River to the Mediterranean Sea. For instance, based on standard
330 values of annual SPM flux of 4-5 M t $yr^{-1}$, Lipiatou and Albaiges (Lipiatou and Albaigés,
331 1994) estimated ~14-18 t $yr^{-1}$ for the annual $\Sigma_{14}$PAH flux of the Rhône River. In the same
332 way, Lipiatou et al. (Lipiatou et al., 1997) evaluated the annual $\Sigma_{11}$PAH flux to ~5-33 t $yr^{-1}$
333 using standard SPM flux values between 2-10 t $yr^{-1}$. These values are coherent with the
334 $\Sigma_{14}$PAH flux of 14 t $yr^{-1}$ assessed by Sicre et al. (2008), using by an annual SPM flux of 13.9
335 M t $yr^{-1}$ for the year 1994-1995. These assessments of HAPs fluxes are between 2- and 11-
336 fold higher than our measurements due in part to the high annual SPM flux values used in
337 these studies. They are up to 2.5-fold higher than our inter-annual average SPM flux (5.5 M t
338 $yr^{-1}$). Similarly, the annual $\Sigma_5$PCB flux estimated by Tronczyński and Héas-Moisan (1996)
339 during the year 1994-1995 is four-fold higher than our estimate. In this case, the $\Sigma_5$PCB flux
340 difference is explained both by the high values of the annual SPM flux (15.8 M t $yr^{-1}$ vs. 5.5

M t $yr^{-1}$ in this study) and the $\Sigma_5$PCB concentrations (35.5 µg $kg^{-1}$ vs. 12.7 µg $kg^{-1}$ in this study) measured by the authors. Always about PCB, the recent study of Dendievel et al (2019) evaluated the inter-annual $\Sigma_5$PCBi budget (2007-2017) of about 97 kg $yr^{-1}$. This overestimation of about 60% higher than our estimate could be attributed to the use of a standard mean $\Sigma_5$PCBi concentration value, rather than a continuous measure of PCBi concentrations during the span of time. Finally, annual TME fluxes are also concerned by such differences in assessment due to the SPM flux estimates. According to Radakovitch et al. (2008) and Ollivier et al. (2011), which calculated an inter-annual SPM flux ~7 M t $yr^{-1}$, the sum of Cr, Co, Ni, Cu, Zn, Cd and Pb fluxes between 2001 and 2003 was about 3,182 t $yr^{-1}$ on average, against 1,720 t $yr^{-1}$ for $\Sigma_7$TME in the present study (Table S1).

At the Rhône river mouth, these studies carried out since the mid-1990s assessing organic and inorganic micropollutant fluxes discharged to the Mediterranean Sea were usually based on limited grab sampling surveys over a full year at best. Such short monitoring periods lead to significant disparities in annual micropollutant fluxes, because they induce an overestimation of the annual SPM flux. Indeed, beyond the different methods used to calculate SPM fluxes discharged to the sea, the high inter-annual variability of SPM fluxes rules out any attempt to assess representative micropollutant fluxes inferred from a single year of SPM monitoring.

A comparison of these micropollutant fluxes at the Rhône River outlet with those discharged to the sea by other large rivers shows significant differences, since PAHs and PCBi fluxes were estimated for the Yangtze River (watershed surface area 1.8 M $km^2$), the Mississippi River (3.3 M $km^2$) and the Saint-Laurent River (1.3 M $km^2$) around, respectively, 365 and 73 t $yr^{-1}$ (~120- and 1200-fold higher, respectively), 160 and 32 t $yr^{-1}$ (~50- and 500-fold higher, respectively), and 25 and 5 t $yr^{-1}$ (~8- and 80-fold higher, respectively) (Liu et al.,

2008). These annual micropollutants fluxes have to be weighted by the catchment size of these rivers to estimate specific fluxes and thus assess their differences of contamination. In this regard, PAHs and PCBi specific fluxes are, respectively, around 73-329 g km² $yr^{-1}$ and 7-73 g km² $yr^{-1}$ (highly above the Rhône River) for the Yangtze River, 17-78 g km² $yr^{-1}$ (similar to the Rhône River) and 1.8-17 g km² $yr^{-1}$ (highly above the Rhône River) for the Mississippi River, and 7-32 g km² $yr^{-1}$ (slightly below the Rhône River) and 0.7-7 g km² $yr^{-1}$ (highly above the Rhône River) for the Saint-Lawrence River.

As consequence, it appears more suitable to compare these fluxes with rivers showing features, such as the size of catchment and numbers of inhabitants, analogous to the Rhône River basin (75,900 km² and 15.5 M inhab). For instance, the inter-annual average $\Sigma_7$PCBi and $\Sigma_{16}$PAH fluxes assessed at the Seine River outlet (78,600 km² and 17.5 M inhab) between the period 2000-2014, with 90 kg $yr^{-1}$ (i.e., around 1 g km² $yr^{-1}$) (Briand et al., 2016) and 2.3 t $yr^{-1}$(i.e., around 30 g km² $yr^{-1}$) (Fisson et al., 2015), respectively, are similar to those of the Rhône River at Beaucaire (i.e., respectively, about 0.8 g km² $yr^{-1}$ and 40 g km² $yr^{-1}$) estimated in the present study (Table S2). These results strengthen the fact that these micropollutants track rather well urbanization and population (i.e., Schwientek et al., 2013; Rügner et al., 2019). In contrast, glyphosate (870 kg $yr^{-1}$ or 11 g km² $yr^{-1}$), AMPA (4,700 kg $yr^{-1}$ or 60 g km² $yr^{-1}$), and $\Sigma_9$TME (323 t $yr^{-1}$ or 4 kg km² $yr^{-1}$) fluxes (Fisson et al., 2015) delivered at the Seine estuary are wholly different from those of the Rhône River at its outlet, with about 97±20 kg $yr^{-1}$ (1.3 g km² $yr^{-1}$), 220±45 kg $yr^{-1}$ (2.9 g km² $yr^{-1}$) and 1,802±152 t $yr^{-1}$ (24 kg km² $yr^{-1}$), respectively (Table S1). Regarding glyphosate and AMPA, such differences could be explain by agricultural activities since they are highly developed in the Seine River basin (Schott et al., 2009), and largely prevailed by cereal cultivation, which is known to resort on glyphosate (Grandcoin et al., 2017). Finally, the geological basements of the Rhône and Seine watersheds

involve contrasting mineralogical compositions that could explain their distinct TME fluxes (Rügner et al., 2019).

### 3.2. Hydro-climatic control of the micropollutant fluxes dynamic: floods as seasonal trigger

The inter-annual and inter-annual monthly SPM and particulate micropollutant fluxes were calculated over the entire period 2008-2018 for the five tributaries monitored, and at the catchment scale (Rhône River at Beaucaire station) (Figs 2, S3 and Table S2). The mean inter-annual SPM flux contributions of the tributaries to the total flux at Beaucaire station are as follows: 31% for the Isère and Durance Rivers, 11% for the Upper Rhône (Jons station), 6% for the Saône River and 0.1% for the Gier River. For the total inter-annual micropollutants flux (all micropollutant families together) released at the Rhône River outlet, the average contributions of the tributaries are the following: 21% for the Isère River, 12% for the Saône River, 10% for the Durance River, 9% for the Upper Rhône (Jons station) and 1% for the Gier River; but these values fluctuate from one micropollutant family to another. Such variability in micropollutant contributions between tributaries is explained by the station-specific chemical fingerprint and SPM flux.

At the Rhône River outlet (Beaucaire station), the evolution of the mean inter-annual monthly micropollutant fluxes is characterized by a tri-modal distribution over the year with maxima centered in (1) November, (2) January, and (3) May-June (Fig. 3). The sum of the micropollutant fluxes exported to the sea during these periods (one third of a year) represents nearly two thirds of the mean inter-annual micropollutant budget of the Rhône River at its outlet. Such a dynamic of the micropollutant fluxes over the year appears to be driven by the hydrological regime of the Rhône River, given the strong positive correlation between water, SPM, and micropollutant (average value used of the Pearson's r computed for all the

415 micropollutants) fluxes at the Rhône River mouth (Pearson's r = 0.98 for SPM vs.
416 micropollutant fluxes (ranging from 0.95 to 1 according to the micropollutants); r = 0.70 for
417 water vs. micropollutant fluxes (ranging from 0.64 to 0.78 according to the micropollutants),
418 and r = 0.70 for SPM vs. water fluxes). The three-mode profile of the inter-annual monthly
419 micropollutant fluxes closely follows the modes of the complex hydrological regime of the
420 Rhône River combining (Fig. 3):

421 - a first Mediterranean component in November accounting for 24% of the mean
422 inter-annual budget of particulate micropollutant fluxes;
423 - a second oceanic pluvial component in January accounting for 15% of the mean
424 inter-annual budget of particulate micropollutant fluxes;
425 - a third nival component in May-June accounting for 24% of the mean inter-annual
426 budget of particulate micropollutant fluxes.

427

428 Such a seasonal behavior of the micropollutant fluxes dynamic of the Rhône River over
429 the year suggests a decisive hydro-climatic control. In this respect, the daily time-series of the
430 water and micropollutant fluxes calculated over the 2008-2018 period show that 70% of the
431 particulate micropollutant fluxes released to the Mediterranean Sea occurred during flood
432 events (defined as half of the 2-year flood peak discharge at Beaucaire; i.e., $Q$ > 2,900 $m^3$ $s^{-1}$)
433 accounting for 11% of the time. These figures are similar to the estimates assessed by
434 Radakovitch et al. (2008) and Ollivier et al. (2011) since they considered ~ 80% of the inter-
435 annual average TME fluxes delivered into the Mediterranean Sea occurs in less than 12% of
436 the time. In comparison, Sicre et al (2008) assessed that 90% of the inter-annual average flux
437 of $\Sigma_{14}$PAH reach the Mediterranean Sea during flood events. Still based on the daily time-
438 series of the micropollutant fluxes, this large micropollutant flux carried by the Rhône River
439 during floods evolves exponentially according to the flood power:

- the last decile of the most powerful floods ($Q$ > 4,500 $m^3$ $s^{-1}$), integrating 1% of time spent, accounts for 28% on average of the total micropollutant fluxes discharged to the sea during the time range of the study (2008-2018);
- floods exceeding the 2-year flood peak discharge ($Q$ > 6,000 $m^3$ $s^{-1}$) (Pont et al., 2002), integrating 0.2% of time spent, account for 11% on average of the total micropollutant fluxes discharged to the sea during the time range of the study (2008-2018).

Based on the mean inter-annual monthly profiles of the micropollutant fluxes of the Rhône River tributaries (Fig. 3), the identification of the sources of the three seasonal modes occurring at the river mouth are easily resolved. In this way, the first Mediterranean component appears to be largely triggered by the micropollutant fluxes coming from the Durance River, which supplies about 19% (ranging from 9% to 40% according to the micropollutant families) of the total micropollutant fluxes released into the sea in November. In comparison, the other tributaries inputs fluctuate between 1.5% (Gier River) and 7% (Saône River) during this period. The second seasonal mode of the micropollutant fluxes observed in January at the Rhône River outlet implies an oceanic pluvial component regulating part of the hydrology of the Saône, Isère and Upper-Rhône basins, which, respectively, provide 18%, 14%, and 10% of the micropollutant fluxes exported to the sea at this time. Finally, the nival component of the micropollutant fluxes, arising in May and June, integrates a further significant contribution from the Isère River accounting for 84 and 34%, respectively. In addition, the Durance River and the Upper Rhône River basin provide each an average of 10% of the micropollutant fluxes delivered to the Mediterranean Sea in May and June (Fig. 3).

This hydro-climatic control of the seasonal micropollutant fluxes dynamic in the Rhône River basin raises the issue of the climate change impacts on the future trends of these fluxes.

Since floods act as the main transport vector of the micropollutant fluxes towards the Mediterranean Sea, it appears essential to focus on the regional patterns of the climatic-change signal in flood discharges (Blöschl et al., 2019). In this end, data from the Explore 2070 project (Chauveau et al., 2013), which estimated the possible impacts of climate change on surface water until the end of the twenty-first century for the whole French hydrographic network, provide insights on the probable evolution of the three periods of micropollutant fluxes discharges into the Mediterranean Sea. At the scale of the Rhône River watershed, but also for the main Rhône River tributaries, the oceanic pluvial component should progress (increasing floods) with the increasing winter discharges (Blöschl et al., 2019; Madsen et al., 2014; Bethemont and Bravard, 2016; Dayon et al., 2018) caused by increasing rainfall between January and March (Chauveau et al., 2013). Conversely, the spring nival component is expected to decrease (decreasing floods) at the Rhône River outlet, and more specifically for the major Alpine tributaries (Upper Rhône River basin and Durance and Isère Rivers), due to the warmer temperatures resulting in earlier and decreasing spring snowmelt floods (Blöschl et al., 2019; Chauveau et al., 2013; Madsen et al., 2014; Bethemont and Bravard, 2016; Dayon et al., 2018). Finally, the Mediterranean component is defined by high-intensity floods following intense precipitation events and affecting especially the small "Cevenol" rivers (right bank, southern tributaries of the Rhône River) (Fig. 1). Recently, Blöschl et al. (2019) estimated that, in a warmer climate, local convective storms might increase in southern Europe and could lead to an increase of the floods magnitude in small watersheds. Typically, we could expect an increase in the fall moisture flux originating from warmer Mediterranean temperatures that would result in increasing Cevenol rivers floods. This assumption is supported by the projection of the 10-year return period flood quantile, using multi-models of changes, which could increase for the Cevenol rivers in the next decades (Sauquet and Lang, 2017). As a result, the Mediterranean component weight would increase. These potential

490 responses of the seasonal behavior of micropollutant fluxes due to the changing climate
491 would result in particulate micropollutant fluxes released into the Mediterranean Sea over a
492 shorter period of time, which would be centered in autumn and winter. As a result, the
493 chemical pollution on the receiving coastal waters would be more intense at this time of year
494 than it currently is.
495
496 **3.3. Defining the chemical cocktails and the overall pollution level to track the spatial**
497 **heterogeneity of large watersheds**

498 In order to define the spatial trends and ranking of the overall contamination level of the
499 six stations studied, a Principal Component Analysis (PCA) was performed on flood versus
500 low flow median concentrations of the 29 quantified substances (Fig. 4A and B). Based on
501 114 tests of Pearson's correlation coefficient performed between the content of particulate
502 organic carbon (POC in g $kg^{-1}$ dry weight) and the 5 PCBi, 13 PAHs and Hg concentrations
503 (mg $kg^{-1}$ dry weight) (micropollutants for which there is an affinity for organic carbon) at the
504 six stations, no micropollutant concentrations-organic content relationship was found. For
505 ~75% of the cases (87 of 114) $r < 0.2$ and p-value $> 0.05$. As a result, the micropollutant
506 concentrations are expressed only on a dry weight (d.w.) basis.

507 The first principal component (F1 ~ 89%) was largely contributed from all
508 micropollutants, meaning that F1 tracks the overall pollution level. Consequently, the F1
509 scores of each station for low flow and flood conditions (Fig. 4A) allow to rank the stations
510 according to their overall contamination level. The resulting first ranking is presented on the
511 X-axis of Fig. 4A, in descending order from right to left, from the Gier River for low flow to
512 the Durance River for flood. In order to ensure the reliability of this classification, two Heat
513 Maps were performed using the same data set (Fig. 4C). The left panel of the figure 4C shows
514 a Heat Map run with all the stations, which are ranked from left to right on the x-axis in a

515 descending order according to their overall pollution level. The resulting classification is
516 similar to that provided by the PCA (Fig. 4A). A third ranking was performed, using land use
517 data for the catchments of the monitoring stations, by summing the anthropized-land use
518 categories (Fig. S1). This third ranking is similar to those obtained by the statistical
519 treatments, except for the Durance and Isère Rivers which are nevertheless very close: Gier
520 (64%) > Saône (63%) > Beaucaire (43%) > Jons (35%) > Durance (23%) > Isère (22%).
521 Based on these classifications of the overall pollution level, three coherent water
522 quality-related groups of stations arise (defined by the clustering analysis of the Heat Maps;
523 see section Statistical analysis of micropollutant concentrations of the Supplementary
524 Material) (Fig. 4C): considered as highly contaminated (Gier and Saône Rivers), intermediate
525 (Beaucaire and Jons stations on the Rhône River), and relatively clean (Isère and Durance
526 Rivers) (Fig. 4). The stations of Jons and Beaucaire display an intermediate level of
527 contamination suggesting the Rhône River waters homogenize efficiently the various
528 contributions of its tributaries. Moreover, the higher overall contamination level of the
529 Beaucaire station compared to the Jons station, both in low flow and flood conditions (Fig.
530 4A and C), demonstrates of a progressive downstream enrichment of the pollution of the
531 Rhône River's waters. Such a spatial trend, with increasing PCB concentrations downstream
532 the Rhône River, has recently been reported by Mourier et al. (2014) using sediment cores
533 from the alluvial plain. This downstream increasing trend of the chemical pollution of the
534 Rhône River's waters could result from the density of the metropolitan areas sheltered in the
535 Rhône Valley downstream to the Jons station (Lyon, Vienne, Valence, Montélimar, and
536 Avignon). This urban density probably act as many potential contamination sources.
537 The ranking of the monitoring stations also provides useful information on the influence
538 of the hydrological conditions on the overall pollution levels. Indeed, for low flow conditions,
539 the Rhône River tributaries are systematically more contaminated than in floods (Fig. 4A and

C), probably as a consequence of a dilution effect resulting from the introduction of "clean SPM" during sustained hydrological events. For the Gier River, this dilution effect in floods is significantly higher than for the other tributaries (Fig. 4A). A possible explanation is that the widespread catchment areas of the main Rhône River tributaries (Saône, Isère and Durance) are able to limit the dilution effect subsequent to the remobilization of contaminated sediments by the erosion and leaching of the floodplain and bank deposits during flood events (Ciszewski and Grygar, 2016; Pavlowsky et al., 2017). Such a flood-induced reworking of inherited sediments is probably less relevant for the Gier River because of the narrowness of its valley bottoms, and the numerous hydraulic facilities (dikes, ripraps, channelization and covered sections) limiting floodplain sedimentation. Finally, the two Rhône River stations show an opposite behavior with a general pollution (i.e., taking into account all micropollutants) increasing in flood conditions (Fig. 4A and C). Therefore, we suppose inherent processes to the Rhône Valley capable of triggering secondary pollution sources occurring during sustained water discharge events and readable through chemical fingerprints.

In order to test this hypothesis, the second step consists to define sub-catchment-specific chemical fingerprints to highlight the major anthropogenic and geographical sources of micropollutant families in the Rhône River catchment, as well as to decipher the composition of the micropollutant fluxes inputs (tributaries) and output (river mouth). The projection of the 29 micropollutants in the factorial plan of the PCA defined by the principal components F2 and F3 distinguishes efficiently the micropollutants families (panel right Fig. 4B). Indeed, in the correlations circle, PAHs are located on the right side, PCBi on the upper left quarter, and TME, glyphosate and AMPA on the lower left quarter. This clustering of micropollutant families is similar to that of the vertical cluster analysis inferred from the Heat Maps (see panel left in Fig. 4C). To ensure the reliability of our conclusions inferred from of the chemical fingerprints (Figs. 4B and C), we compared them to the station-specific chemical

spectrum (Fig. S4). Hence, for low flow conditions, the chemical cocktails recognized are as follows:

- Beaucaire: PCB, TME and glyphosate/AMPA;
- Jons: PAH and TME (Cu, Cd, Zn);
- Saône: PAH and TME (As, Hg, Pb, Cd);
- Gier: PCB, TME and glyphosate/AMPA;
- Isère: TME and AMPA;
- Durance: no specific chemical fingerprint identified.

The chemical cocktails of the Gier, Beaucaire and Jons stations change towards prevailing PAHs fingerprints during flood condition. This is especially striking for the Beaucaire station experiencing mirror-shape chemical fingerprints (Fig. 4C-right and S4C). Indeed, during floods the TME, glyphosate and AMPA concentrations decrease in favor of PAHs (Fig. 4C-right and S4C). The activation of this secondary source of contamination during floods is probably caused by runoff over artificial areas (Blanchard et al., 2001; Bigus et al., 2014; Froger et al., 2019), which are more widespread in the three catchments involved (Fig. S1). This diffuse source of PAHs is probably triggered when floods are combined with intense precipitation events (David et al., 2012). For both Rhône River stations, this leaching process over artificial surfaces could explain the higher PAHs contamination level during flood periods (Fig. 4B and C-right, S4C and S4E). Indeed, $\Sigma_{13}$PAH concentrations at the Beaucaire and Jons stations increase, respectively, from 444 to 651 µg $kg^{-1}$ (+ 47%), and from 499 to 569 µg $kg^{-1}$ (+ 14%) (Tab. S1). This increase of $\Sigma_{13}$PAH concentrations during floods does not affect the Gier River (see the left Heat Map in Fig. 4C and Table S2) because the dilution effect of this river is more effective than the PAHs inputs during floods.

In order to decipher the pollution source of PAHs in the Rhône River SPM, the most frequently used PAHs molecular diagnostic ratios, i.e., Fla/(Fla+Pyr), BaA/(BaA+Chry) and IndP/(IndP+BghiP) (e.g., Froger et al., 2019; Yunker et al., 2002; Ravindra et al., 2008), were investigated (Fig. S5). Firstly, based on these PAHs ratios, all the monitoring stations show similar fingerprints characterized by a restricted PAHs space implying a common-source of PAHs for the Rhône River SPM. Secondly, these PAHs fingerprints fit that of the runoff particles collected by Gaspéri et al. (2017, 2018) from a storm sewer of the densely urbanized catchment of Sucy (south-east of Paris in France) (Fig. S5). In this respect, as recently suggested by Froger et al. (2019) for the Orge River SPM (catchment located in the Seine River basin), runoff particles would be the main direct PAHs source in the urbanized areas of the Rhône River basin. Thirdly, while atmospheric particles are known to be sensitive to the fossil fuel combustion (Froger et al., 2019) derived from vehicular emissions (Keyte et al., 2016) or household heating (Motelay-Massei et al., 2003), runoff particles-derived pollution source of the Rhône River SPM is mainly composed of mixed vehicular, and biomass combustion emissions, as well as of a minor contribution from fossil fuel combustion (Fig. S5). Finally, this investigation based on two levels of PAHs fingerprints (direct local sources and general combustion origins) evidences that urban runoff is the main direct PAHs source of the Rhône River SPM, which encompasses multiple origins including biomass and fossil fuel combustion. These results are in good agreement with the general statement that urban pressure, population density, and PAHs concentrations in SPM are positively correlated (i.e., Schwientek et al., 2013; Rügner et al., 2019; Parajulee et al., 2017; Poulier et al., 2019).

### 3.4. Exploring the micropollutant missing sources

The inter-annual and inter-annual monthly micropollutant budgets at the Rhône River outlet (Beaucaire station) were computed and compared to the micropollutant fluxes inputs from the tributaries (Figs. 2 and S3). We consider that the negative imbalance (i.e., deficit

budget) is related to the missing sources of micropollutants including non-monitored tributaries, wastewater effluents, runoff over artificial areas, as well as remobilization of highly contaminated sediments subsequent to the erosion and leaching of the floodplain, and bank deposits during flood events (e.g., Ciszewski and Grygar, 2016; Pavlowsky et al., 2017; Poulier et al., 2019). These missing sources constitute about 47% on average, and more specifically about 65% for $\Sigma_5$PCB, 54% for $\Sigma_{13}$PAH, 60% for glyphosate, 24% for AMPA, and 31% for $\Sigma_9$TME of the total annual flux of micropollutants (Figs. 2 and S3). Because these values are greater than the inter-annual SPM deficit (21%), this implies that the missing sources have higher particulate micropollutant concentrations. In order to remove the influence of SPM flux variations, SPM-flux-averaged micropollutant mean concentrations, called thereafter "total concentration", were calculated to improve the assessment of the missing sources magnitude, as well as their identification. The total concentration $C_{total,j}$ of a micropollutant $j$ from $n$ inputs (or tributaries) is the sum of the partial concentrations $C_{partial,j}$ of the inputs to the system:

$$C_{total,j} = \frac{\sum_{i=1}^{n} F_{i,j}}{\sum_{i=1}^{n} F_{i,SPM}} = \sum_{i=1}^{n} C_{partial,j} \quad (1)$$

$$\text{with } C_{partial,j} = \frac{F_{i,j}}{\sum_{i=1}^{n} F_{i,SPM}} \quad (2)$$

$F_{i,j}$: flux of micropollutant $j$ from input $i$

$F_{i,SPM}$: flux of SPM from input $i$

Analogous to partial pressures in a mixture of gases, the "partial concentration" of an input is the notional concentration of that input if the micropollutants alone were diluted in the entire SPM flux of all the inputs. Then, we compared the inter-annual and inter-annual

monthly $C_{total,j}$ of the inputs to that one output of the system at the Rhône River outlet (Beaucaire station) for:

$$C_{output,j} = \frac{F_{output,j}}{F_{output,SPM}} \quad (3)$$

with $F_{output,j}$: flux of micropollutant $j$ from *output*

$F_{output,SPM}$: flux of SPM from *output*

Results of $C_{total,j}$, $C_{partial,j}$ and $C_{output,j}$in figures 2 and S6 are expressed in terms of tributaries contributions (%) to be consistent with SPM and micropollutant fluxes, as well as to facilitate the comparison of the inputs micropollutant "total concentration" ($C_{total,j}$) vs. output micropollutant concentration ($C_{output,j}$). By measuring the positive (excess) or the negative (deficit) difference between $C_{output,j}$ and $C_{total,j}$, we can assess the presence and the relative degree of contamination of the micropollutant missing sources. Regarding that, two groups of micropollutants can be distinguished at the inter-annual scale (Figs 2 and S6). The first one refers to the PCBi, PAHs and glyphosate, and shows a significant negative imbalance (large deficit) because their inter-annual deficit is between 28% and 51%. The second one encompasses AMPA and TME, which show a minor negative imbalance (small deficit), because their inter-annual deficit is between 1% and 13%. Such low deficits highlight low micropollutant concentrations of the missing sources.

In order to facilitate the identification of the missing sources of contamination, we performed an inter-annual monthly decomposition of the $C_{partial,j}$ (tributaries inputs) relative to the $C_{output,j}$ (Rhône River outlet, Beaucaire station) for all micropollutants (Fig. 5 and S7). The inter-annual monthly distribution of the total $\Sigma_{13}$PAH concentrations relative to the output $\Sigma_{13}$PAH concentrations shows an irregular trend over the year with the highest deficits in April (36%), May (46%), June (50%), and November (58%). This temporal pattern is

consistent with the rainiest months of the Rhône Valley (Météo France), which shelter numerous metropolitan areas (Lyon, Vienne, Valence, Montélimar, and Avignon). The main missing sources of the total $\Sigma_{13}$PAH concentrations should be triggered by precipitation-induced runoff, and leaching over artificial surfaces of the Rhône valley's urban areas. This potential and non-exclusive missing urban source of PAHs concentrations is finding support in Becouze-Lareure et al. (2019) showing that stormwater is the most important source of PAHs at the outlet of two urban catchments in the Lyon metropolitan area. According to the uncertainty analysis, the inter-annual deficit of the SPM-flux-averaged PAHs mean concentrations of about 28% (Fig.5) is explained for 41% by the relative uncertainty of the PAHs missing source concentration (see the supplementary text).

In contrast, the inter-annual monthly profile of the total $\Sigma_5$PCB concentrations relative to the output $\Sigma_5$PCB concentrations (Figs 5 and S7) is steady over the year, with a mean deficit of about 51%, except for October (only about 10%), due to a very high contribution from the Upper-Rhône River (56%). This sudden increasing of the Upper-Rhône River contribution has to be considered as an artefact resulting from a deliberate or accidental isolated discharge of PCBi into the Upper Rhône River waters. Indeed, an exceptionally high value of PCBi concentration measured (two-fold higher than the low flow median concentration) was found in SPM collected in October 2013 (PCBi concentrations were measured two times on the same sample to check for the absence of analytical bias). The unchanging profile of the total $\Sigma_5$PCB concentrations over the year could express the presence of a single, permanent, and relatively highly contaminated source of PCBi. According to the recent sediment-cores investigation led by Liber et al. (2019) on subsurface PCB-contaminated sediments along the Rhône River's alluvial margins, surface sediments deposited to a maximum depth of 25 cm from the topographic level (time window > 2005) downstream of the city of Lyon show elevated PCBi concentrations. The $\Sigma_5$PCB

concentration is on average about 42±12 µg $kg^{-1}$ (76±29 µg $kg^{-1}$ for the time window > 1968) in these easiest remobilized sediments induced by floodplain surface leaching during flood events (Ciszewski and Grygar, 2016).

In order to test the reliability of this potential missing source of PCBi, the assessment of the SPM flux released from the alluvial margins to fill alone the inter-annual PCB-flux deficit was estimated. The SPM flux $F_{k,SPM}$ of a missing source $k$ with assumed concentration $C_{k,j}$ in micropollutant $j$ can be computed as:

$$F_{k,SPM} = \frac{F_{k,j}}{C_{k,j}} \quad (4)$$

$$\text{with } F_{k,j} = F_{output,j} - \sum_{i=1}^{n} F_{i,j} \quad (5)$$

Therefore, considering an inter-annual PCB-flux deficit of about 40 kg (Table S1) and a mean PCB concentration of 42 µg $kg^{-1}$ in the subsurface stored sediments of the Rhône River's alluvial margins (Liber et al., 2019), this potential missing source of contamination should then supply a SPM flux of 0.95 Mt $yr^{-1}$ to fill alone the inter-annual PCB-flux deficit. Although such a value may appear high in view of the mean inter-annual SPM flux at Beaucaire (about 17%) (Table S1), it falls within the range of errors of the inter-annual SPM flux measurement at the Rhône River outlet commonly considered <±20% (Horowitz, 2003). As a result, this estimated figure of the SPM flux inputs required to fill alone the inter-annual PCB-flux deficit shows that the alluvial margins are a convincing missing source of PCBi in the Rhône River basin. This missing source of PCBi is all the more convincing that the inter-annual deficit of the SPM-flux-averaged PCBi mean concentrations of about 51% (Fig.5) is explained for 21% by the relative uncertainty of the PCBi concentration (see the supplementary text) of the subsurface stored sediments of the Rhône River's alluvial margins.

704 The inter-annual monthly profiles of the total glyphosate and AMPA concentrations
705 relative to the output glyphosate and AMPA concentrations (Figs 5 and S7) exhibit significant
706 differences leading to distinct mean monthly deficits about 46% and 1%, respectively.
707 Because AMPA is, among other, a glyphosate degradation product, they usually co-occur in
708 the environment (Aparicio et al., 2013; Lupi et al., 2015), so it was expected to observe a
709 similar monthly co-evolution over the year. According to the literature reviewed by
710 Grandcoin et al. (2017) about glyphosate and AMPA in the streams, a few factors lead to
711 accelerate degradation rates of glyphosate. These include the sorption capacity of soils, which
712 depends in turn to clay, organic matter, and Al-Fe oxides and hydroxides contents, and the
713 total metal concentrations in soils and water. A particular focus on the partial glyphosate and
714 AMPA concentrations of the inputs reveals an overall similar proportion for these two
715 molecules for each tributary, except for the Isère River marked by a disproportionate mean
716 monthly partial concentration reaching 47% of the output AMPA concentration against 10%
717 for glyphosate (Fig 5). By removing this surplus of AMPA coming from the Isère River, the
718 general profiles of the total glyphosate and AMPA concentrations of inputs over the year is
719 similar to that of $\Sigma_{13}$PAH. Consequently, their highest deficits, recorded from May until
720 November (Fig 5), could result from the same urban missing sources located in the Rhône
721 valley downstream of the city of Lyon. Indeed, in addition to agricultural leachates, AMPA
722 and glyphosate have an urban wastewater effluents source (e.g., Grandcoin et al., 2017;
723 Kolpin et al., 2006; Botta et al., 2009), for which releases are particularly substantial during
724 heavy rainfall runoff (Botta et al., 2009; Hanke et al., 2010).

725 Finally, the inter-annual monthly mean deficit between the output TME concentrations
726 and their total concentrations of inputs is much lower than for the other micropollutant
727 families, since it is around 13%. This figure should be considered with caution as large
728 differences are observed between TME that could be sorted in two groups as follows (Fig. 5):

- Zn, Ni, Cu, Cr, Co, and As display a mean inter-annual monthly deficit of about 10% (ranging from 5 to 15%), which is explained for 36% on average (ranging from 27 to 48%) by the relative uncertainty of this TME cluster's missing source concentration;
- Pb, Hg, and Cd display a mean inter-annual monthly deficit of about 26% (ranging from 25 to 28%), which is explained for 25% on average (ranging from 21 to 31%) by the relative uncertainty of this TME cluster's missing source concentration.

As expected, the largest partial TME concentrations of the inputs are coming from the Isère River, with an average contribution to the total TME concentrations over the year of about 36%. (Fig. 2). This figure is higher for the first TME group (40%), than the second group (28%). In view of these differences, we assume that the main TME missing sources are highly enriched in Pb, Hg, and Cd in the one hand, and slightly less for Zn, Ni, Cu, Cr, Co, and As, on the other hand. In addition, the co-evolution of the total Pb, Cd and Hg concentrations of the inputs over the year indicates a triggering of their main missing source from September to November, since the greatest deficits of the TME concentrations inputs occurred at this time (Figs. 5 and S6). This information builds a strong body of evidence toward the non-monitored Cevenol tributaries (Eyrieux, Ardèche, Cèze and Gard rivers, Fig. 1), as the main sought missing source, because they are known to be highly enriched in TME coming from the remobilization of former mining sites tailings (Pb/Zn mining districts, and coal production districts) (Resongles et al., 2014, 2015). To ensure the reliability of this missing source, we compared the Cevenol tributaries' SPM fluxes ($F_{k,SPM}$) needed to fill the inter-annual TME-flux deficits ($F_{k,j}$), with the inter-annual SPM flux deficit (~ 1.1 Mt $yr^{-1}$) (Table S1). We used a mean concentration of the Cevenol tributaries $C_{k,j}$ (Ardèche, Gard and Cèze) (Fig. 1) of 93.3 mg $kg^{-1}$ for Pb, 0.05 mg $kg^{-1}$ for Hg, 0.82 mg $kg^{-1}$ for Cd, 211.4 mg $kg^{-1}$ for Zn, 35.7 mg $kg^{-1}$ for Ni, 46.4 mg $kg^{-1}$ for Cu, 80.7 mg $kg^{-1}$ for Cr, 14.9 mg $kg^{-1}$ for Co, and

44.5 mg $kg^{-1}$ for As (data from the Rhône Sediment Observatory). The Cevenol tributaries' SPM fluxes ($F_{k,SPM}$) were estimated at around 1.1 Mt $yr^{-1}$ (ranging from 0.5-1.5 Mt $yr^{-1}$ according to the TME considered and more specifically 0.9 Mt $yr^{-1}$ for Pb and Cd), with the exception of Hg with 4 Mt $yr^{-1}$. Therefore, we suggest that the Cevenol tributaries constitute the main missing source of TME fluxes, except for Hg, since the estimated SPM flux ($F_{k,SPM}$) is equal to the inter-annual SPM flux deficit.

## 4. Conclusions and perspectives

Based on the Rhône Sediment Observatory, a one-of-a-kind monitoring network, we have explored the seasonal dynamic of land-based organic and inorganic particulate-bound micropollutant fluxes, which appears to be controlled by the complex hydrological regime of the Rhône River. The inter-annual monthly distribution of the micropollutant fluxes released into the Mediterranean Sea displays a three-mode profile related to the Mediterranean, oceanic pluvial, and nival floods acting as the primary transport vector. Face to climate change, the major part of micropollutants fluxes would reach the Mediterranean Sea during a single shorter period centered in autumn and winter. Original multi-variate statistical analysis methods integrating median concentrations of a large number of micropollutants highlighted the spatial heterogeneity of watersheds in terms of the overall micropollutant concentrations, land use and chemical cocktails. Finally, based on a SPM-flux-averaged micropollutant concentrations mass balance of the system and the estimates of the relative uncertainty of the missing source concentration, we tried to identify the missing sources of micropollutants in the Rhône River watershed. We assume that the potential missing sources of PAHs, PCBi and TME (only for Pb and Cd) would be, respectively, the metropolitan areas and the alluvial margins of the Rhône River valley, and the unmonitored Cevenol tributaries.

From this research emerge perspectives relating to the potential interactions between the micropollutant fluxes dynamic, climate change, river-floodplain connectivity, river restoration programs and legacy contaminated sediments. For the past twenty years the river restoration and management programs of the Rhône River include the reactivation of channel side arms, and the removal of lateral embankments in order to reinstate lateral connectivity between the channel and its alluvial margins (e.g., Provansal et al., 2012; Bravard and Gaydou, 2015; Riquier et al., 2015). However, without an accurate assessment of the contamination levels of the sedimentary volumes stored on the margins, these actions could lead to the reintroduction into the system of inherited sediments highly contaminated because of their remobilization (Provansal et al., 2012; Delile et al., 2014; Bravard and Gaydou, 2015; Eschbach et al., 2018). This issue is even more sensitive that the river engineering could positively interact with the climate change-enhanced flood magnitude. Indeed, improving the river-floodplain connectivity would facilitate the propagation of the increased flood discharges towards the alluvial margins and strengthening their ability to remobilize contaminated legacy deposits on floodplains. To that purpose, it would be useful to resort to sediment cores to evaluate micropollutant volumes stored, as well as their chemical composition. Still based on sediment cores, they could be used as archives of past SPM and particulate micropollutant fluxes (Ferrand et al., 2012; Cossa et al., 2018) able to fill the gap between recent measurements from the monitoring station network and past fluxes. Such a perspective would provide a pluri-secular historical depth to the spatial and temporal trajectories of the development of the urban societies.

## Acknowledgments

This study was conducted within the Rhône Sediment Observatory (OSR), a multi-partner research program funded through the Plan Rhône by the European Regional Development

Fund (ERDF), Agence de l'eau RMC, CNR, EDF and three regional councils (Auvergne-Rhône-Alpes, PACA and Occitanie). We are grateful to the following Irstea colleagues for SPM sampling, field campaigns, sample treatment, chemical analysis, data analysis, and GIS analysis: Alexandra Gruat, Ghislaine Grisot, Hélène Angot, Mickaël Lagouy, Marina Launay, Benjamin Renard, Aymeric Dabrin, and André Chandesris. We also thank Julie Gattacceca from the CEREGE laboratory, and Hugo Lepage from the IRSN laboratory for field sampling, SPM sampling, and preparation for the southern OSR stations.

## References

AFNOR, 2000. XP X33–012 - Characterisation of Sludges - Determination of Polynuclear Aromatic Hydrocarbons (PAH) and Polychlorinated Biphenyls (PCB) - Caractérisation des boues.

Al Rajab, A. J., 2007. Impact sur l'environnement d'un herbicide non sélectif, le glyphosate Approche modélisée en conditions contrôlées et naturelles. PhD thesis, University of Lorraine, France, 169 p.

Antonelli, C., Eyrolle, F., Rolland, B., Provansal, M., Sabatier, F., 2008. Suspended sediment and 137Cs fluxes during the exceptional December 2003 flood in the Rhone River, southeast France. Geomorphology 95, 350–360.

Aparicio, V.C., De Gerónimo, E., Marino, D., Primost, J., Carriquiriborde, P., Costa, J.L., 2013. Environmental fate of glyphosate and aminomethylphosphonic acid in surface waters and soil of agricultural basins. Chemosphere 93, 1866–1873.

Baylis AD. 2000. Why glyphosate is a global herbicide: strengths, weaknesses and prospects. Pest Management Science 56, 299-308.

Beckie, H. J., Flower, K. C., Ashworth, M. B., 2020. Farming without Glyphosate? Plants 96, 15 p.

Becouze-Lareure, C., Dembélé, A., Coquery, M., Cren-Olivé, C., Bertrand-Krajewski, J.-L., 2019. Assessment of 34 dissolved and particulate organic and metallic micropollutants discharged at the outlet of two contrasted urban catchments. Science of The Total Environment 651, 1810–1818.

Bethemont, J., Bravard, J.-P., 2016. Pour saluer le Rhône. Libel, Lyon, France.

Bigus, P., Tobiszewski, M., Namieśnik, J., 2014. Historical records of organic pollutants in sediment cores. Marine Pollution Bulletin 78, 26–42.

Blanchard, M., Teil, M.-J., Ollivon, D., Garban, B., Chestérikoff, C., Chevreuil, M., 2001. Origin and distribution of polyaromatic hydrocarbons and polychlorobiphenyls in urban effluents to wastewater treatment plants of the paris area (FRANCE). Water Research 35, 3679–3687.

Blichert-Toft, J., Delile, H., Cin-Ty, L., Stos-Gale, Z., Billström, K., Andersen, T., Hannu, H., Albarède, F., 2016. Large-scale tectonic cycles in Europe revealed by distinct Pb isotope provinces. Geochem Geophys Geosyst 17, 3854–3864.

Blöschl, G., Hall, J., Viglione, A., Perdigão, R.A.P., Parajka, J., Merz, B., Lun, D., Arheimer, B., Aronica, G.T., Bilibashi, A., Boháč, M., Bonacci, O., Borga, M., Čanjevac, I.,

Castellarin, A., Chirico, G.B., Claps, P., Frolova, N., Ganora, D., Gorbachova, L., Gül, A., Hannaford, J., Harrigan, S., Kireeva, M., Kiss, A., Kjeldsen, T.R., Kohnová, S., Koskela, J.J., Ledvinka, O., Macdonald, N., Mavrova-Guirguinova, M., Mediero, L., Merz, R., Molnar, P., Montanari, A., Murphy, C., Osuch, M., Ovcharuk, V., Radevski, I., Salinas, J.L., Sauquet, E., Šraj, M., Szolgay, J., Volpi, E., Wilson, D., Zaimi, K., Živković, N., 2019. Changing climate both increases and decreases European river floods. Nature 573, 108–111.

Botta, F., Lavison, G., Couturier, G., Alliot, F., Moreau-Guigon, E., Fauchon, N., Guery, B., Chevreuil, M., Blanchoud, H., 2009. Transfer of glyphosate and its degradate AMPA to surface waters through urban sewerage systems. Chemosphere 77, 133–139.

Bravard, J.-P., 2018. Crises sédimentaires du globe. 1, Grands cours d'eau, de l'abondance à la rareté, Collection Géosciences. ISTE éditions, London.

Bravard, J.-P., Gaydou, P., 2015. Historical Development and Integrated Management of the Rhône River Floodplain, from the Alps to the Camargue Delta, France, in: Hudson, P.F., Middelkoop, H. (Eds.), Geomorphic Approaches to Integrated Floodplain Management of Lowland Fluvial Systems in North America and Europe. Springer New York, New York, NY, pp. 289–320.

Briand, C., Gateuille, D., Gasperi, J., Moreau-Guigon, E., Alliot, F., Chevreuil, M., Blanchard, M., Teil, M.-J., Brignon, J.-M., Labadie, P., Budzinski, H., Rocher, V., Azimi, S., Thevenot, D., Moilleron, R., Meybeck, M., Mouchel, J.-M., 2016. Bilans et flux de polluants organiques dans le bassin de la Seine (PIREN-Seine No. phase VII).

Chauveau, M., Chazot, S., Perrin, C., Bourgin, P.-Y., Sauquet, E., Vidal, J.-P., Rouchy, N., Martin, E., David, J., Norotte, T., Maugis, P., Lacaze, X.D., 2013. Quels impacts des changements climatiques sur les eaux de surface en France à l'horizon 2070 ? La Houille Blanche 5–15.

Chong, J., Wishart, D.S., Jianguo, X., 2019. Using MetaboAnalyst 4.0 for Comprehensive and Integrative Metabolomics Data Analysis. Current Protocols in Bioinformatics 68, e86.

Ciszewski, D., Grygar, T.M., 2016. A Review of Flood-Related Storage and Remobilization of Heavy Metal Pollutants in River Systems. Water Air Soil Pollut 227, 239.

Cossa, D., Fanget, A.-S., Chiffoleau, J.-F., Bassetti, M.-A., Buscail, R., Dennielou, B., Briggs, K., Arnaud, M., Guédron, S., Berné, S., 2018. Chronology and sources of trace elements accumulation in the Rhône pro-delta sediments (Northwestern Mediterranean) during the last 400years. Progress in Oceanography, Special issue of MERMEX project: Recent advances in the oceanography of the Mediterranean Sea 163, 161–171.

Dachs, J., Lohmann, R., Ockenden, W.A., Méjanelle, L., Eisenreich, S.J., Jones, K.C., 2002. Oceanic Biogeochemical Controls on Global Dynamics of Persistent Organic Pollutants. Environ. Sci. Technol. 36, 4229–4237.

David, A., Bancon-Montigny, C., Salles, C., Rodier, C., Tournoud, M.-G., 2012. Contamination of riverbed sediments by hazardous substances in the Mediterranean context: Influence of hydrological conditions. Journal of Hydrology 468–469, 76–84.

Dayon, G., Boé, J., Martin, É., Gailhard, J., 2018. Impacts of climate change on the hydrological cycle over France and associated uncertainties. Comptes Rendus Geoscience 350, 141–153.

Delile, H., Blichert-Toft, J., Goiran, J.-P., Keay, S., Albarède, F., 2014. Lead in ancient Rome's city waters. Proc. Natl. Acad. Sci. U.S.A. 111, 6594–6599.

Dendievel, A.-M., Mourier, B., Coynel, A., Evrard, O., Labadie, P., Ayrault, S., Debret, M., Koltalo, F., Copard, Y., Faivre, Q., Gardes, T., Vauclin, S., Budzinski, H., Grosbois, C., Winiarski, T., and Desmet, M.: Spatio-temporal assessment of the PCB sediment contamination in the four main French River Basins (1945–2018). Earth Syst. Sci.

Data Discuss, in review, 2019.
E.C, 2000. Directive 2000/60/EC of the European Parliament and of the Council of 23 October 2000 Establishing a Framework for Community Action in the Field of Water Policy. OJ L 327, 22.12.2000. pp. 1–73.
E.C., 2011. Guidance Document No. 27. Technical Guidance For Deriving Environmental Quality Standards, Technical Report for Common Implementation Strategy for the Water Framework Directive (2000/60/EC)- 2011-055. 204 p.
Eschbach, D., Schmitt, L., Imfeld, G., May, J.-H., Payraudeau, S., Preusser, F., Trauerstein, M., Skupinski, G., 2018. Long-term temporal trajectories to enhance restoration efficiency and sustainability on large rivers: an interdisciplinary study. Hydrology and Earth System Sciences 22, 2717–2737. https://doi.org/10.5194/hess-22-2717-2018
Ferrand, E., Eyrolle, F., Radakovitch, O., Provansal, M., Dufour, S., Vella, C., Raccasi, G., Gurriaran, R., 2012. Historical levels of heavy metals and artificial radionuclides reconstructed from overbank sediment records in lower Rhône River (South-East France). Geochimica et Cosmochimica Acta, Environmental Records of Anthropogenic Impacts 82, 163–182.
Fisson, C., 2015. Flux en contaminants à l'estuaire de la Seine (Etude réalisée par le GIP Seine-Aval).
Froger, C., Ayrault, S., Gasperi, J., Caupos, E., Monvoisin, G., Evrard, O., Quantin, C., 2019. Innovative combination of tracing methods to differentiate between legacy and contemporary PAH sources in the atmosphere-soil-river continuum in an urban catchment (Orge River, France). Science of The Total Environment 669, 448–458.
Gaspéri, J., Ayrault, S., Moreau-Guigon, E., Alliot, F., Labadie, P., Budzinski, H., Blanchard, M., Muresan, B., Caupos, E., Cladière, M., Gateuille, D., Tassin, B., Bordier, L., Teil, M.-J., Bourges, C., Desportes, A., Chevreuil, M., Moilleron, R., 2018. Contamination of soils by metals and organic micropollutants: case study of the Parisian conurbation. Environ Sci Pollut Res 25, 23559–23573.
Gasperi, J., Sébastian, C., Ruban, V., Delamain, M., Percot, S., Wiest, L., Mirande, C., Caupos, E., Demare, D., Kessoo, M.D., Saad, M., Schwartz, J.J., Dubois, P., Fratta, C., Wolff, H., Moilleron, R., Chebbo, G., Cren, C., Millet, M., Barraud, S., Gromaire, M.-C., 2017. Contamination des eaux pluviales par les micropolluants : avancées du projet INOGEV. TSM 51–70.
Gioia, R., Dachs, J., Nizzetto, L., Berrojalbiz, N., Galba, C., Del Vento, S., Méjanelle, L., Jones, K.C., 2011. Sources, Transport and Fate of Organic Pollutants in the Oceanic Environment, in: Persistent Pollution – Past, Present and Future. M. Quante, R. Ebinghaus, G. Flöser, pp. 111–139.
Gómez-Gutiérrez, A.I., Jover, E., Bodineau, L., Albaigés, J., Bayona, J.M., 2006. Organic contaminant loads into the Western Mediterranean Sea: estimate of Ebro River inputs. Chemosphere 65, 224–236.
Grandcoin, A., Piel, S., Baurès, E., 2017. AminoMethylPhosphonic acid (AMPA) in natural waters: Its sources, behavior and environmental fate. Water Research 117, 187–197.
Hanke, I., Wittmer, I., Bischofberger, S., Stamm, C., Singer, H., 2010. Relevance of urban glyphosate use for surface water quality. Chemosphere 81, 422–429.
Horowitz, A., 2003. An evaluation of sediment rating curves for estimating suspended sediment concentrations for subsequent flux calculations - Horowitz - 2003 - Hydrological Processes - Wiley Online Library. Hydrological Processes 17, 3387–3409.
Horowitz, A.J., 2009. Monitoring suspended sediments and associated chemical constituents in urban environments: lessons from the city of Atlanta, Georgia, USA Water Quality Monitoring Program. J Soils Sediments 9, 342–363.

Keyte, I.J., Albinet, A., Harrison, R.M., 2016. On-road traffic emissions of polycyclic aromatic hydrocarbons and their oxy- and nitro- derivative compounds measured in road tunnel environments. Science of The Total Environment 566–567, 1131–1142.

Kolpin, D.W., Thurman, E.M., Lee, E.A., Meyer, M.T., Furlong, E.T., Glassmeyer, S.T., 2006. Urban contributions of glyphosate and its degradate AMPA to streams in the United States. Sci. Total Environ 354, 191–197.

Lade, S.J., Steffen, W., de Vries, W. et al. 2020. Human impacts on planetary boundaries amplified by Earth system interactions. Nat Sustain 3, 119–128.

Launay, M., 2014. Flux de matières en suspension, de mercure et de PCB particulaires dans le Rhône, du Léman à la Méditerranée. Université Claude Bernard - Lyon I, Lyon.

Launay, M., Dugué, V., Faure, J.-B., Coquery, M., Camenen, B., Le Coz, J., 2019. Numerical modelling of the suspended particulate matter dynamics in a regulated river network. Science of The Total Environment 665, 591–605.

Lepage, H., Masson, M., Delanghe, D., Le Bescond, C., 2019. Grain size analyzers: results of an intercomparison study. SN Appl. Sci. 1, 1100.

Liber, Y., Mourier, B., Marchand, P., Bichon, E., Perrodin, Y., Bedell, J.-P., 2019. Past and recent state of sediment contamination by persistent organic pollutants (POPs) in the Rhône River: Overview of ecotoxicological implications. Science of The Total Environment 646, 1037–1046.

Lipiatou, E., Albaigés, J., 1994. Atmospheric deposition of hydrophobic organic chemicals in the northwestern Mediterranean Sea: comparison with the Rhone river input. Marine Chemistry, 12th International Symposium @'Chemistry of the Mediterranean@' 46, 153–164.

Lipiatou, E., Tolosa, I., Simó, R., Bouloubassi, I., Dachs, J., Marti, S., Sicre, M.-A., Bayona, J.M., Grimalt, J.O., Saliott, A., Albaiges, J., 1997. Mass budget and dynamics of polycyclic aromatic hydrocarbons in the Mediterranean Sea. Deep Sea Research Part II: Topical Studies in Oceanography 44, 881–905.

Liu, K.-K., Seitzinger, S., Mayorga, E., Harrison, J., Ittekkot, V., 2009. Fluxes of Nutrients and Selected Organic Pollutants Carried by Rivers, in: Watersheds, Bays and Bounded Seas: The Science and Management of Semi-Enclosed Marine Systems, SCOPE. Urban, E. R., Sundby, B., Malanotte-Rizzoli, P., and Melillo, J., Island Press, Washington, DC, pp. 141–167.

Ludwig, W., Dumont, E., Meybeck, M., Heussner, S., 2009. River discharges of water and nutrients to the Mediterranean and Black Sea: Major drivers for ecosystem changes during past and future decades? Progress in Oceanography 80, 199–217.

Lupi, L., Miglioranza, K.S.B., Aparicio, V.C., Marino, D., Bedmar, F., Wunderlin, D.A., 2015. Occurrence of glyphosate and AMPA in an agricultural watershed from the southeastern region of Argentina. Sci. Total Environ. 536, 687–694.

Madsen, H., Lawrence, D., Lang, M., Martinkova, M., Kjeldsen, T.R., n.d. Review of trend analysis and climate change projections of extreme precipitation and floods in Europe. Journal of Hydrology 519, 3634–3650.

Malaj, E., Ohe, P.C. von der, Grote, M., Kühne, R., Mondy, C.P., Usseglio-Polatera, P., Brack, W., Schäfer, R.B., 2014. Organic chemicals jeopardize the health of freshwater ecosystems on the continental scale. PNAS 111, 9549–9554.

Masson, M., Angot, H., Le Bescond, C., Launay, M., Dabrin, A., Miège, C., Le Coz, J., Coquery, M., 2018. Sampling of suspended particulate matter using particle traps in the Rhône River: Relevance and representativeness for the monitoring of contaminants. Sci. Total Environ. 637–638, 538–549.

Meyer, T., Lei, Y.D., Muradi, I., Wania, F., 2009. Organic Contaminant Release from Melting Snow. 1. Influence of Chemical Partitioning. Environmental Science &

Technology 43, 657–662.
Météo France. Public administrative establishment for meteorology and climatology in France. http://www.meteofrance.com/accueil
Meybeck, M., 2003. Global analysis of river systems: from Earth system controls to Anthropocene syndromes. Philos Trans R Soc Lond B Biol Sci 358, 1935–1955.
Moatar, F., Meybeck, M., Raymond, S., Coynel, A., Ludwig, W., Mano, V., Nemery, J., Poirel, A., Etcheber, H., Crouzet, P., 2008. Evaluation des flux de MES à partir des suivis discrets : méthodes de calcul et incertitudes. La Houille Blanche 64–71.
Motelay-Massei, A., Ollivon, D., Garban, B., Chevreuil, M., 2003. Polycyclic aromatic hydrocarbons in bulk deposition at a suburban site: assessment by principal component analysis of the influence of meteorological parameters. Atmospheric Environment 37, 3135–3146.
Mourier, B., Desmet, M., Van Metre, P.C., Mahler, B.J., Perrodin, Y., Roux, G., Bedell, J.-P., Lefèvre, I., Babut, M., 2014. Historical records, sources, and spatial trends of PCBs along the Rhône River (France). Sci. Total Environ. 476–477, 568–576.
Ollivier, P., Radakovitch, O., Hamelin, B., 2011. Major and trace element partition and fluxes in the Rhône River. Chemical Geology 285, 15–31.
Parajulee, A., Lei, Y.D., Kananathalingam, A., McLagan, D.S., Mitchell, C.P.J., Wania, F., 2017. The transport of polycyclic aromatic hydrocarbons during rainfall and snowmelt in contrasting landscapes. Water Research 124, 407–414.
Pavlowsky, R.T., Lecce, S.A., Owen, M.R., Martin, D.J., 2017. Legacy sediment, lead, and zinc storage in channel and floodplain deposits of the Big River, Old Lead Belt Mining District, Missouri, USA. Geomorphology 299, 54–75.
Pont, D., Simonnet, J.-P., Walter, A.V., 2002. Medium-term Changes in Suspended Sediment Delivery to the Ocean: Consequences of Catchment Heterogeneity and River Management (Rhône River, France). Estuarine, Coastal and Shelf Science 54, 1–18.
Poulier, G., Launay, M., Le Bescond, C., Thollet, F., Coquery, M., Le Coz, J., 2019. Combining flux monitoring and data reconstruction to establish annual budgets of suspended particulate matter, mercury and PCB in the Rhône River from Lake Geneva to the Mediterranean Sea. Sci. Total Environ. 658, 457–473.
Provansal, M., Raccasi, G., Monaco, M., Robresco, S., Dufour, S., 2012. La réhabilitation des marges fluviales, quel intérêt, quelles contraintes ?Le cas des annexes fluviales du Rhône aval. Méditerranée. Revue géographique des pays méditerranéens / Journal of Mediterranean geography 85–94.
Qi, W., Müller, B., Pernet-Coudrier, B., Singer, H., Liu, H., Qu, J., Berg, M., 2014. Organic micropollutants in the Yangtze River: Seasonal occurrence and annual loads. Science of The Total Environment 472, 789–799.
Radakovitch, O., Roussiez, V., Ollivier, P., Ludwig, W., Grenz, C., Probst, J.-L., 2008. Input of particulate heavy metals from rivers and associated sedimentary deposits on the Gulf of Lion continental shelf. Estuarine, Coastal and Shelf Science, Land Ocean Interactions in the Coastal Zone, LOICZ: Lessons from Banda Aceh, Atlantis, and Canute 77, 285–295.
Ravindra, K., Sokhi, R., Van Grieken, R., 2008. Atmospheric polycyclic aromatic hydrocarbons: Source attribution, emission factors and regulation. Atmospheric Environment 42, 2895–2921.
Resongles, E., Casiot, C., Freydier, R., Dezileau, L., Viers, J., Elbaz-Poulichet, F., 2014. Persisting impact of historical mining activity to metal (Pb, Zn, Cd, Tl, Hg) and metalloid (As, Sb) enrichment in sediments of the Gardon River, Southern France. Sci. Total Environ. 481, 509–521.
Resongles, E., Casiot, C., Freydier, R., Le Gall, M., Elbaz-Poulichet, F., 2015. Variation of

dissolved and particulate metal(loid) (As, Cd, Pb, Sb, Tl, Zn) concentrations under varying discharge during a Mediterranean flood in a former mining watershed, the Gardon River (France). Journal of Geochemical Exploration 158, 132–142.

Riquier, J., Piégay, H., Michalková, M.S., 2015. Hydromorphological conditions in eighteen restored floodplain channels of a large river: linking patterns to processes. Freshwater Biology 60, 1085–1103.

Rockström, J., Steffen, W., Noone, K., Persson, A., Chapin, F.S., Lambin, E.F., Lenton, T.M., Scheffer, M., Folke, C., Schellnhuber, H.J., Nykvist, B., de Wit, C.A., Hughes, T., van der Leeuw, S., Rodhe, H., Sörlin, S., Snyder, P.K., Costanza, R., Svedin, U., Falkenmark, M., Karlberg, L., Corell, R.W., Fabry, V.J., Hansen, J., Walker, B., Liverman, D., Richardson, K., Crutzen, P., Foley, J.A., 2009. A safe operating space for humanity. Nature 461, 472–475.

Rügner, H., Schwientek, M., Milačič, R., Zuliani, T., Vidmar, J., Paunović, M., Laschou, S., Kalogianni, E., Skoulikidis, N.T., Diamantini, E., Majone, B., Bellin, A., Chiogna, G., Martinez, E., López de Alda, M., Díaz-Cruz, M.S., Grathwohl, P., 2019. Particle bound pollutants in rivers: Results from suspended sediment sampling in Globaqua River Basins. Sci. Total Environ. 647, 645–652.

Sadaoui, M., Ludwig, W., Bourrin, F., Raimbault, P., 2016. Controls, budgets and variability of riverine sediment fluxes to the Gulf of Lions (NW Mediterranean Sea). Journal of Hydrology 540, 1002–1015.

Sauquet, E., Lang, M., 2017. 18 - Flood Regimes: Recent Development and Future Under Climate Change, in: Vinet, F. (Ed.), Floods. Elsevier, pp. 299–309.

Schott, C., Mignolet, C., Benoît, M., 2009. Découvrir l'agriculture du bassin de la Seine pour comprendre les enjeux de la gestion de l'eau. Agence de l'Eau Seine-Normandie (No. 5), Piren-Seine.

Schulze, T., Ricking, M., Schröter-Kermani, C., Körner, A., Denner, H.-D., Weinfurtner, K., Winkler, A., Pekdeger, A., 2007. The German Environmental Specimen Bank. J Soils Sediments 7, 361–367.

Schwientek, M., Rügner, H., Beckingham, B., Kuch, B., Grathwohl, P., 2013. Integrated monitoring of particle associated transport of PAHs in contrasting catchments. Environ. Pollut. 172, 155–162.

Sicre, M.-A., Fernandes, M.B., Pont, D., 2008. Poly-aromatic hydrocarbon (PAH) inputs from the Rhône River to the Mediterranean Sea in relation with the hydrological cycle: Impact of floods. Marine Pollution Bulletin 56, 1935–1942.

Steffen, W., Richardson, K., Rockström, J., Cornell, S.E., Fetzer, I., Bennett, E.M., Biggs, R., Carpenter, S.R., de Vries, W., de Wit, C.A., Folke, C., Gerten, D., Heinke, J., Mace, G.M., Persson, L.M., Ramanathan, V., Reyers, B., Sörlin, S., 2015. Sustainability. Planetary boundaries: guiding human development on a changing planet. Science 347, 736–746.

Syvitski, J.P.M., Kettner, A.J., 2007. On the flux of water and sediment into the Northern Adriatic Sea. Continental Shelf Research, Sediment Dynamics in the Western Adriatic Sea 27, 296–308.

Syvitski, J.P.M. and Saito, Y., 2007. Morphodynamics of deltas under the influence of humans. Glob. Planet. Changes 57, 261–282.

Syvitski, J.P.M., Vörösmarty, C.J., Kettner, A.J., Green, P., 2005. Impact of humans on the flux of terrestrial sediment to the global coastal ocean. Science 308, 376–380.

Thollet, F., Le Bescond, C., Lagouy, M., Gruat, A., Grisot, G., Le Coz, J., Coquery, M., Lepage, H., Gairoard, S., Gattacceca, J., Ambrosi, J.-P., Radakovitch, O., 2018. Observatoire des Sédiments du Rhône. Irstea.

Tronczyński, J., Héas-Moisan, K., 1996. Evaluation des charges polluantes du Rhône à la

Méditerranée. Contaminants organiques organoazotés et organochlorés dissous et particulaires dans le Rhône (Etude Agence de l'Eau Rhône Méditerranée Corse), Ifremer.
UNEP, 2001. Final Act of the Plenipotentiaries on the Stockholm Convention on Persistent Organic Pollutants. United Nations Environment Program Chemicals, Geneva, Switzerland.
UNEP/MAP, 2003. Riverine transport of water, sediments and pollutants to the Mediterranean Sea (Technical Reports No. 141). Athens.
United Nations (1998) Protocol to the 1979 Convention on Long-Range Transboundary Air Pollution on Persistent Organic Pollutants. ECE/EB.AIR/60
U.S. EPA, 1998. Method 7473 (SW-846): Mercury in Solids and Solutions by Thermal Decomposition, Amalgamation, and Atomic Absorption Spectrophotometry. Washington, DC.
Walling, D.E., Owens, P.N., Carter, J., Leeks, G.J.L., Lewis, S., Meharg, A.A., Wright, J., 2003. Storage of sediment-associated nutrients and contaminants in river channel and floodplain systems. Applied Geochemistry 18, 195–220.
Wang, J.-Z., Guan, Y.-F., Ni, H.-G., Luo, X.-L., Zeng, E.Y., 2007. Polycyclic Aromatic Hydrocarbons in Riverine Runoff of the Pearl River Delta (China): Concentrations, Fluxes, and Fate. Environ. Sci. Technol. 41, 5614–5619.
Yang, X., Wang, F., Bento, C.P.M., Meng, L., van Dam, R., Mol, H., Liu, G., Ritsema, C.J., Geissen, V., 2015. Decay characteristics and erosion-related transport of glyphosate in Chinese loess soil under field conditions. Sci. Total Environ. 530-531, 87-95.
Yunker, M.B., Macdonald, R.W., Vingarzan, R., Mitchell, R.H., Goyette, D., Sylvestre, S., 2002. PAHs in the Fraser River basin: a critical appraisal of PAH ratios as indicators of PAH source and composition. Organic Geochemistry 33, 489–515.

## Figure captions

**Fig. 1.** Map of the Rhône River basin with its main tributaries and the monitoring stations for water discharge, suspended particulate matter and associated micropollutants.

**Fig. 2.** Inter-annual and inter-annual monthly water, SPM and micropollutant budgets (plain colors) and partial/total (sum of partial) micropollutant concentrations (pale colors) relative to the Rhône River outlet (orange line, Beaucaire station) (in %). The contributions of the monitored tributaries to the budgets and to the total concentrations are shown for each family of micropollutants.

**Fig. 3.** Inter-annual monthly water, SPM and micropollutant fluxes over the 2008-2018 period at each monitoring station. Organic and inorganic micropollutant fluxes are expressed

in kilograms and tons by year, respectively. Listing of abbreviations of micropollutants detailed in Table S1 and S2.

**Fig. 4.** Statistical analysis of the median concentrations for all the micropollutants at all the monitoring stations, for low flow and flood conditions: Principal Component Analysis (panels A and B for factors F1/F2 and F2/F3, respectively) and Heat Maps (panel C) whose columns and rows are arranged according to a hierarchical cluster analysis. The left Heat Map in the panel C includes all the monitoring stations, while the right one is performed without the Gier River to improve the readability of the results of the other stations. The arrows in the panel B depict the prevailing PAHs fingerprint during flood conditions for the Gier and Beaucaire stations. Listing of abbreviations of micropollutants detailed in Table S1 and S2.

**Fig. 5.** Decomposition of the inter-annual monthly total micropollutant concentrations relative to the Rhône River outlet (orange line, Beaucaire station) (in %). The contributions of the partial micropollutant concentrations of the monitored tributaries are displayed for each family of micropollutants.

**Figure**

Click here to download high resolution image

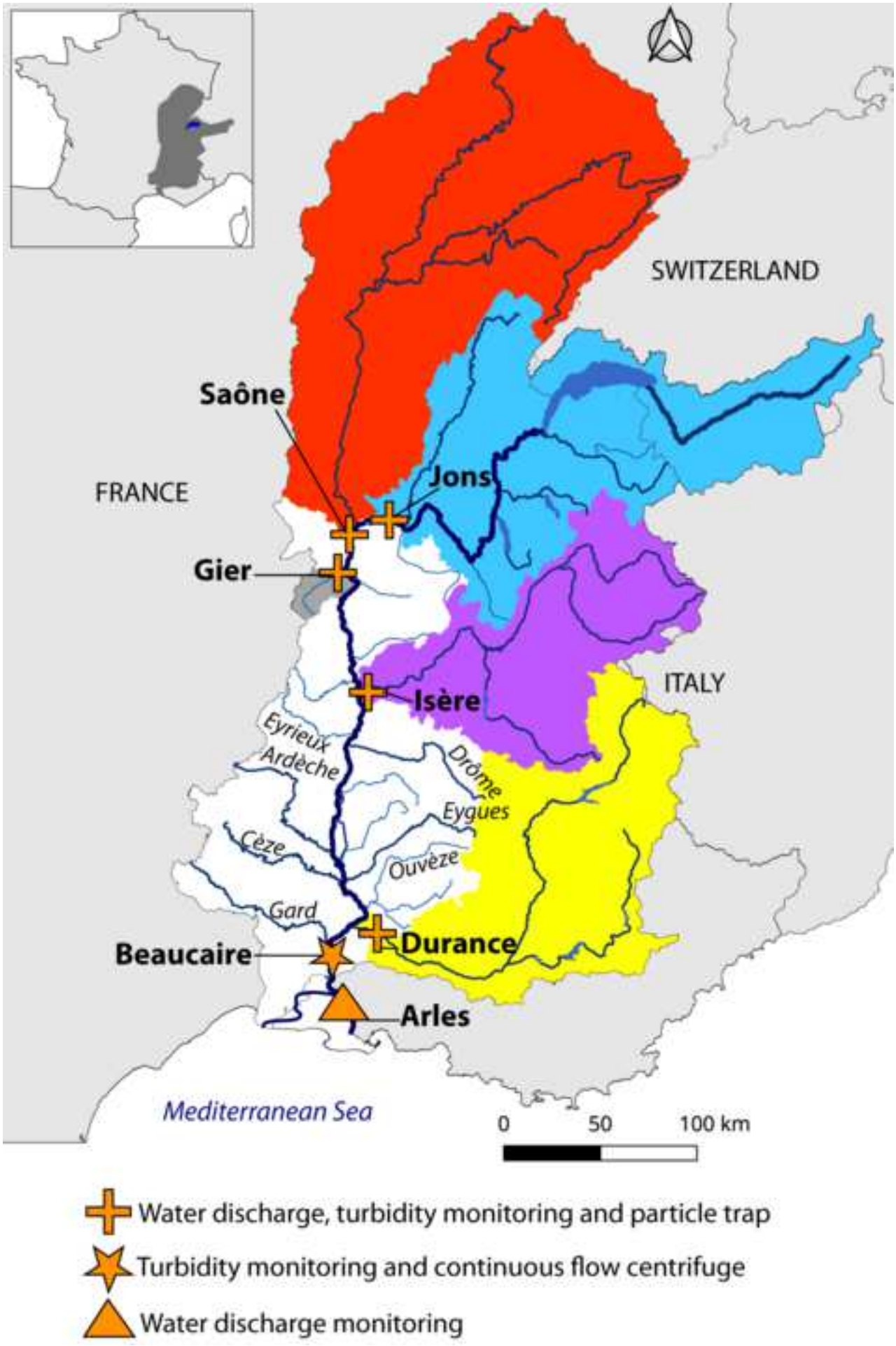

Figure

Click here to download high resolution image

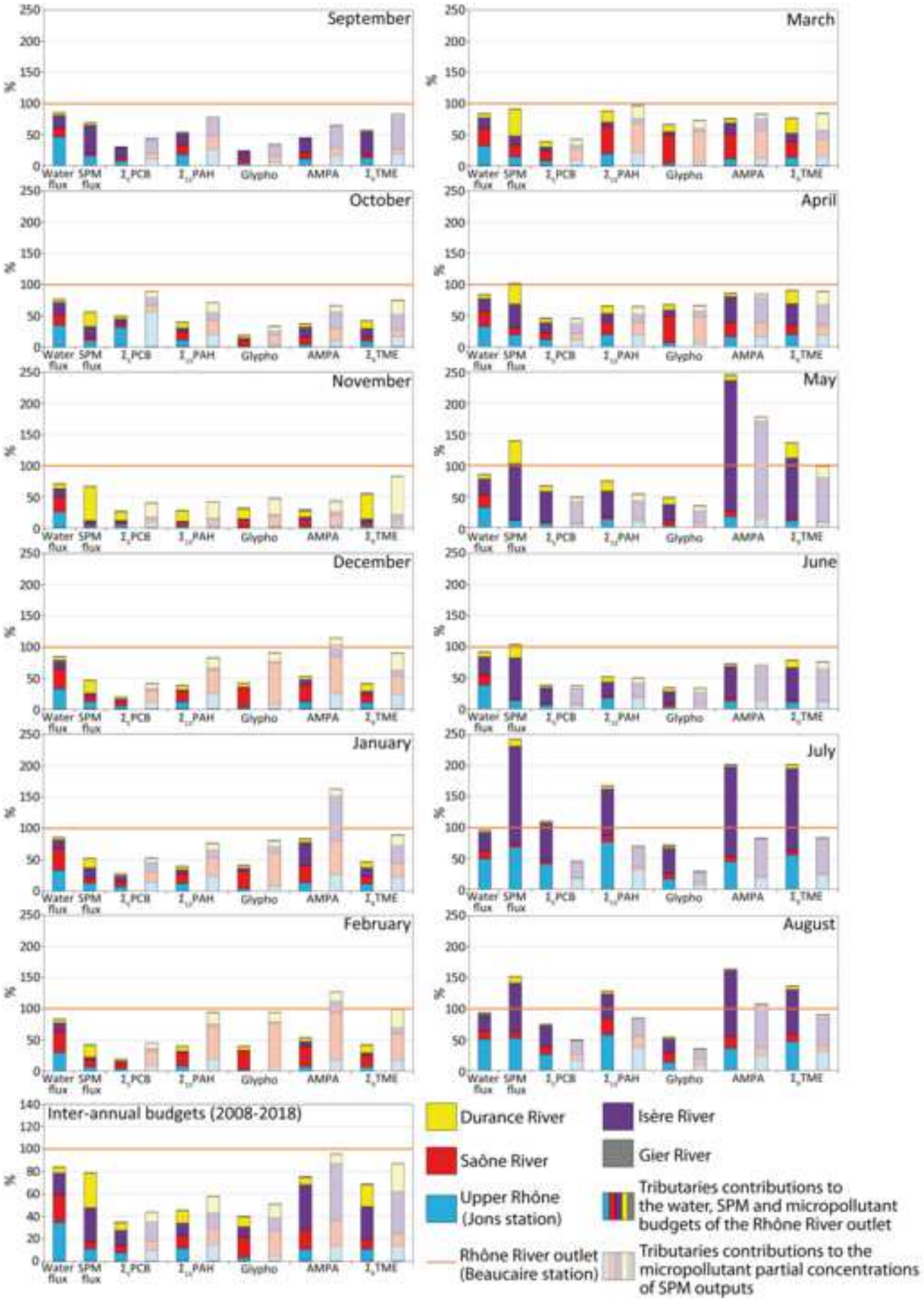

**Figure**

**Click here to download high resolution image**

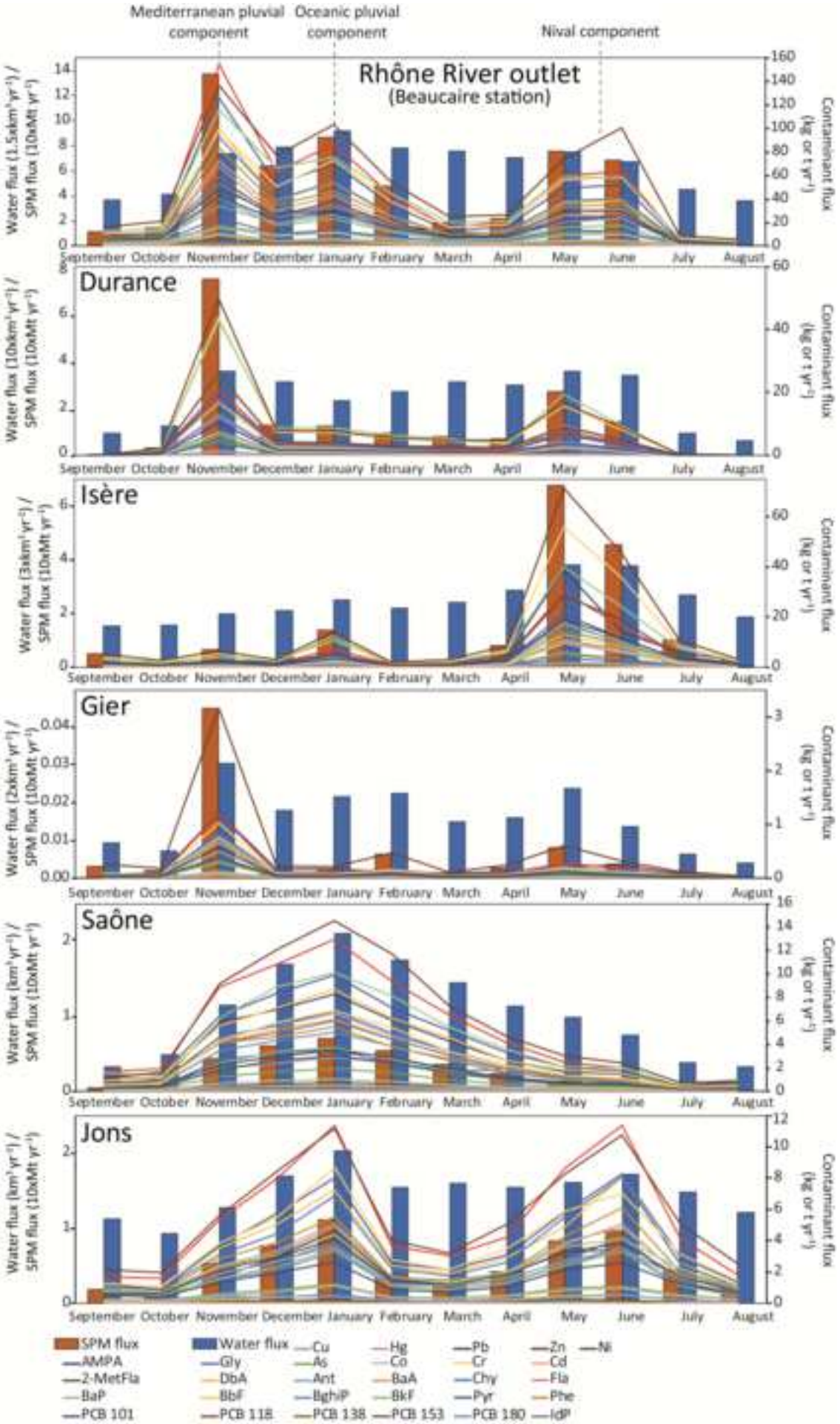

Figure

Click here to download high resolution image

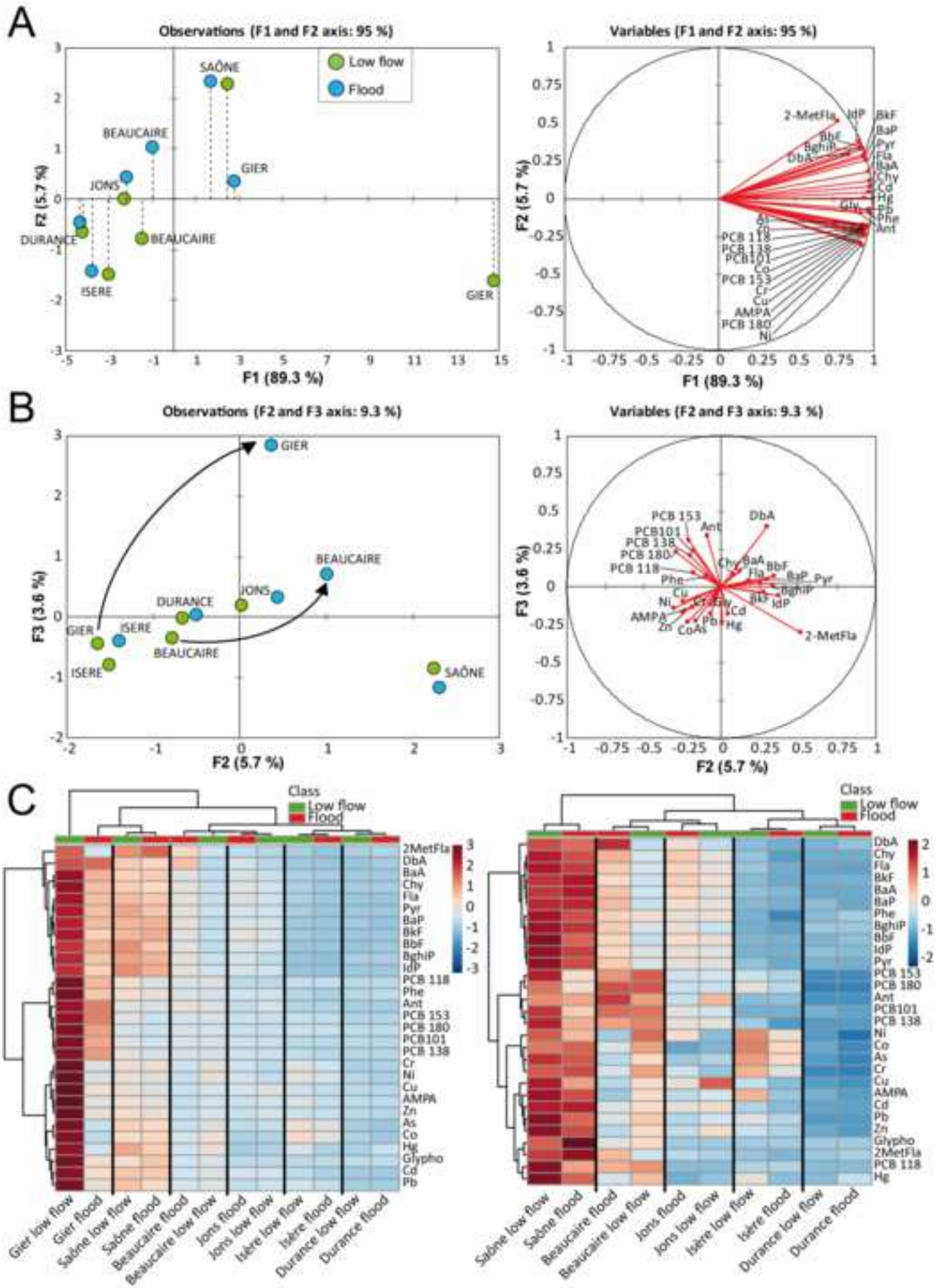

Figure

Click here to download high resolution image